Earth, Planets and Space

FULL PAPER Open Access

Evaluation and analysis of the precipitable water vapor in Inner Mongolia of China

Qi Bai[1], Qiaoli Kong[1,2,3*], Xiaolong Mi[2], Wu Chen[2], Junsheng Ding[2], Yunqing Huang[1], Meiqi Li[4] and Qian Li[1]

Abstract

The Inner Mongolia Autonomous Region is an ecological protective screen in the northern part of China. The precipitable water vapor (PWV) products with high precision and spatiotemporal resolution are critical for climate research in this region. This study aims to comprehensively evaluate and analyze the PWV in Inner Mongolia using the global navigation satellite system (GNSS), radiosonde (RS), the fifth-generation European Center for Medium-Range Weather Forecasts Reanalysis (ERA5), and the Second Modern-Era Retrospective Analysis for Research and Applications (MERRA-2) data. The comparison between GNSS PWV and RS PWV reveals an average bias of −0.68 mm and a root mean square error (RMSE) of 2.17 mm, indicating the high accuracy of GNSS PWV and its potential as an assessment tool of other PWV products. In comparison to PWV of GNSS, PWV of ERA5 and MERRA-2 exhibit an annual average bias of 0.17 and 0.39 mm, respectively, and an annual average RMSE of 1.63 and 2.99 mm, respectively. The monthly average bias and RMSE of ERA5 are 0.41 and 1.79 mm, respectively, while those of MERRA-2 are 0.43 and 3.05 mm, respectively. In the Inner Mongolia region, the diurnal anomaly variation range of PWV for all three datasets is stable within −0.6–0.6 mm. The evaluation results demonstrate that PWV retrieved by ERA5 and MERRA-2 are applicable in the Inner Mongolia region, with ERA5 showing better consistency with GNSS PWV. This study provides valuable insights for understanding the formation, patterns, monitoring, and warning of meteorological natural disasters in the Inner Mongolia region.

Keywords PWV, GNSS, ERA5, MERRA-2, Inner Mongolia region

*Correspondence:
Qiaoli Kong
kqlabc3334@163.com
Full list of author information is available at the end of the article

Graphical Abstract

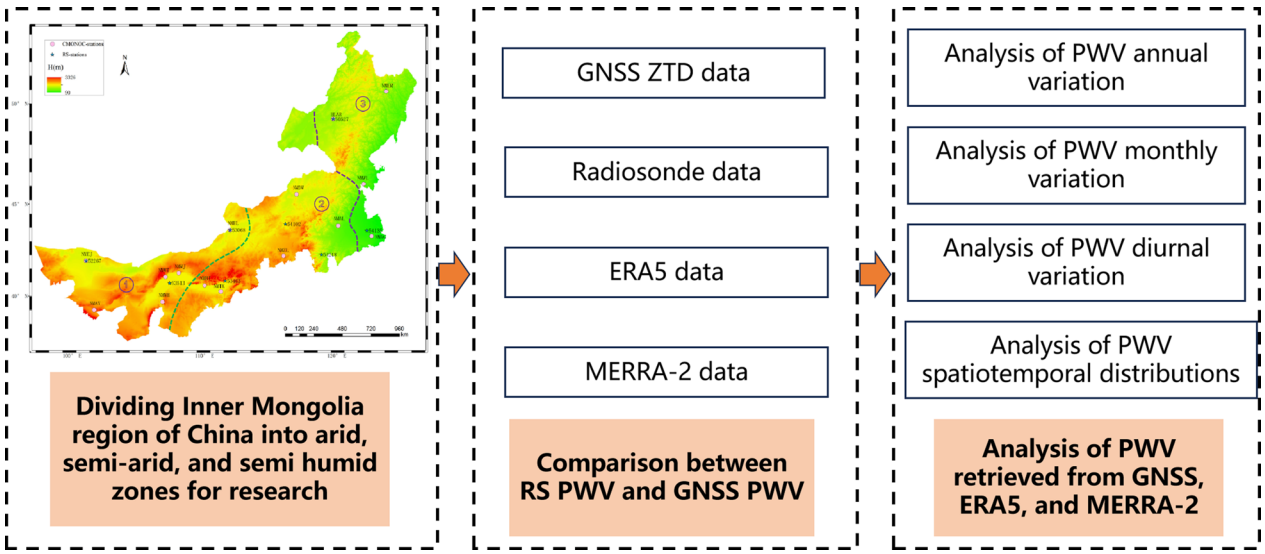

1 Introduction

The Inner Mongolia Autonomous Region, located in the inland area of the Northern Hemisphere mid-latitudes in China, serves as an important ecological protective screen in northern China. It is characterized by diverse and complex terrain, primarily composed of plateaus separated by mountains along the edges. Being far from the ocean, it experiences diverse types of climate, which mainly belong to temperate continental climate. The unique terrain conditions in Inner Mongolia contribute to the formation of a special climate, resulting in frequent meteorological disasters in the region. Water vapor, despite making only up about 4% of the atmosphere, is indispensable to human activities and daily life (Rocken et al. 1997; Colman 2003; Allan and Soden 2008). At the same time, atmospheric water vapor plays a vital role in shaping and developing severe weather events such as heavy rainfall, cold waves, typhoons, severe droughts, and floods (Frank 1977; Zhang et al. 2018b; Huang et al. 2021a). Therefore, conducting comprehensive monitoring of atmospheric water vapor and studying its underlying patterns hold immense significance for understanding the evolution of various extreme weather events and providing early warning for natural disasters (He et al. 2019). The climate in Inner Mongolia is complex and varied, and accurate precipitable water vapor (PWV) data is crucial for improving the accuracy of weather and climate forecasting in the region. Studying the changes in PWV can help understand the characteristics of regional climate change and provide scientific basis for addressing climate change. By analyzing and comparing the performance of different datasets, valuable references can be provided for improving forecasting models and enhancing navigation and positioning accuracy.

PWV is widely used as a prevalent parameter to indicate atmospheric water vapor content and plays a pivotal role in climate research (King et al. 1992). Currently, there are many technologies to monitor PWV content, including radiosonde (RS), microwave radiometers, satellite remote sensing, etc. (Zeng et al. 2019). Among those techniques, RS stands out as one of the most precise methods for PWV detection. However, it is expensive, has low temporal resolution of observation data, and has scarce observation stations, making it challenging to capture spatiotemporal changes in water vapor effectively (Wang and Zhang 2008). Microwave radiometers, radar, and satellite remote sensing techniques have limitations in detection accuracy under certain weather conditions, which restricts their application in meteorological research (Dalu 1986; Gui et al. 2017). Bevis et al. (1992) introduced the idea of global navigation satellite system (GNSS) meteorology, emphasizing the benefits of GNSS technology, including its ability for all-weather observation and high precision. GNSS technology has been widely developed in PWV inversion and detection (Niell et al. 2001). However, in regions with uneven and sparse distribution of GNSS stations, the application of GNSS

PWV in climate monitoring and weather prediction is limited (Xu et al. 2022).

Through the continuous development and improvement of atmospheric reanalysis datasets, these datasets integrate data from diverse sources, including radiosonde and satellite remote sensing measurements. Atmospheric reanalysis datasets offer decades of uninterrupted atmospheric observations that can serve as alternative data for estimating large-scale PWV through PWV inversion (Huang et al. 2021b). GNSS-derived PWV data can be used as valuable validation, while the Crustal Movement Observation Network of China (CMONOC) data has not been combined into atmospheric reanalysis datasets and offers high accuracy and temporal resolution. Generally, it is considered an independent observational source for evaluating PWV derived from some reanalysis data (Li et al. 2003; Huang et al. 2022b). Several research institutions, including the National Aeronautics and Space Administration (NASA) and the European Centre for Medium-Range Weather Forecasts (ECMWF), provide users with the most up-to-date global atmospheric numerical forecast reanalysis products, such as the Modern-Era Retrospective Analysis for Research and Applications, version 2 (MERRA-2), and the ECMWF Fifth Generation global climate reanalysis dataset (ERA5) (Gelaro et al. 2017; Hersbach et al. 2020). Nevertheless, reanalysis data are subject to uncertainties caused by errors in the observation system, numerical forecast models, assimilation schemes, and homogenization processes (Zhao et al. 2010). Therefore, it is necessary to verify the reliability of these products for different regions (Mo et al. 2021).

Numerous researchers have conducted studies on the suitability of several reanalysis datasets using RS PWV and GNSS PWV. Wang et al. (2020) assessed the global scale accuracy of PWV for the five reanalysis datasets using GNSS PWV, and proved that the annual average root mean square error (RMSE) of ERA5 was of the best accuracy with only 1.8 mm. Bock and Parracho (2019) carried out the comparison between the PWV calculated from ERA-Interim reanalysis data with PWV retrieved from 120 IGS stations, and achieved the daily standard deviation below 2 mm. Zhang et al. (2019a) carried out a systematic evaluation of the appropriateness of meteorological parameters obtained from ERA5 for hourly PWV inversion using GPS data in China in 2016. Subsequently, Ssenyunzi et al. (2020) conducted a similar study on ERA5 in East Africa. Huang et al. (2022a) performed an overall assessment of hourly ERA5 PWV and MERRA-2 PWV utilizing GNSS observations of 339 GNSS stations and ground-based meteorological observations in China. The results indicated that both reanalysis datasets are suitable for China. Regarding local regions, Huang et al. (2021b) and Liu et al. (2023) evaluated the applicability of ERA5 PWV and MERRA-2 PWV products using GNSS PWV in the Tibetan Plateau (TP) region and Xinjiang region of China, respectively, and the results showed high accuracy. Xu et al. (2022) qualitatively analyzed the spatiotemporal relationship between PWV of ERA5 and MERRA-2 and precipitation in heavy rain for Zhengzhou, China, using reanalysis data and meteorological stations.

However, the above studies have mainly put emphasis on analyzing the performance of PWV products of different reanalysis datasets for different regions (Wang et al. 2017), with few studies specifically examining the PWVs retrieved from reanalysis data in the Inner Mongolia region of China. This region is of unique geographical importance, with complex and diverse terrain and climate conditions, and serves as an important ecological protective screen. Therefore, this study will thoroughly evaluate and analyze the PWV in the Inner Mongolia region, analyze the differences and consistencies between PWV from different datasets, investigate the annual, monthly, and diurnal anomaly variations of PWV, and deeply study the PWV spatiotemporal variation patterns in different arid/humid zones. This study also provides new data support and scientific basis for meteorological forecasting, geodetic surveying, and regional development in Inner Mongolia. To achieve the goal, the research will partition Inner Mongolia into different arid/humid zones (such as semi-humid, semi-arid, and arid zones), and comprehensively study the spatiotemporal variations of PWV from ERA5 and MERRA-2 for these different zones. GNSS PWV inversion is performed with the zenith tropospheric delay (ZTD) of 15 GNSS stations from CMONOC in Inner Mongolia, and the PWV is applied as the reference value for PWV retrieved by other datasets. The PWV data of four radiosonde stations located in Inner Mongolia is adopted to evaluate the accuracy and reliability of GNSS PWV. A detailed analysis ise conducted on the spatiotemporal factors that affect the accuracy of reanalysis data calculations. The PWV inverted from GNSS, ERA5, and MERRA-2 in different arid/humid regions will be systematically evaluated and compared.

The study is arranged as follows. Section 2 introduces the experimental data, calculation methods, and accuracy evaluation metrics. Section 3 compares the PWV of RS and GNSS PWV in detail, assesses the dependability of GNSS PWV, examines the consistency between PWV of GNSS, ERA5, and MERRA-2, and evaluates their suitability for the Inner Mongolia region. Section 4 explains the conclusions.

2 Data and methods

2.1 Data

To conduct a comprehensive analysis of the accuracy, distribution characteristics, and spatiotemporal variation patterns of the retrieved PWV in the Inner Mongolia, the region has been divided into arid, semi-arid, and semi-humid zones on the basis of the characteristics of precipitation and evaporation of this region (Zhao et al. 2022), as shown in Fig. 1. The data utilized includes GNSS observation data, RS data, ERA5 and MERRA-2 data. The basic information of these data is provided in Table 1, while the station distributions of GNSS and RS are illustrated in Fig. 1. The time range for each type of data is from 2019 to 2021, totaling 3 years. There are data gaps in GNSS and RS datasets, and these missing data will not be taken into consideration to ensure the validity

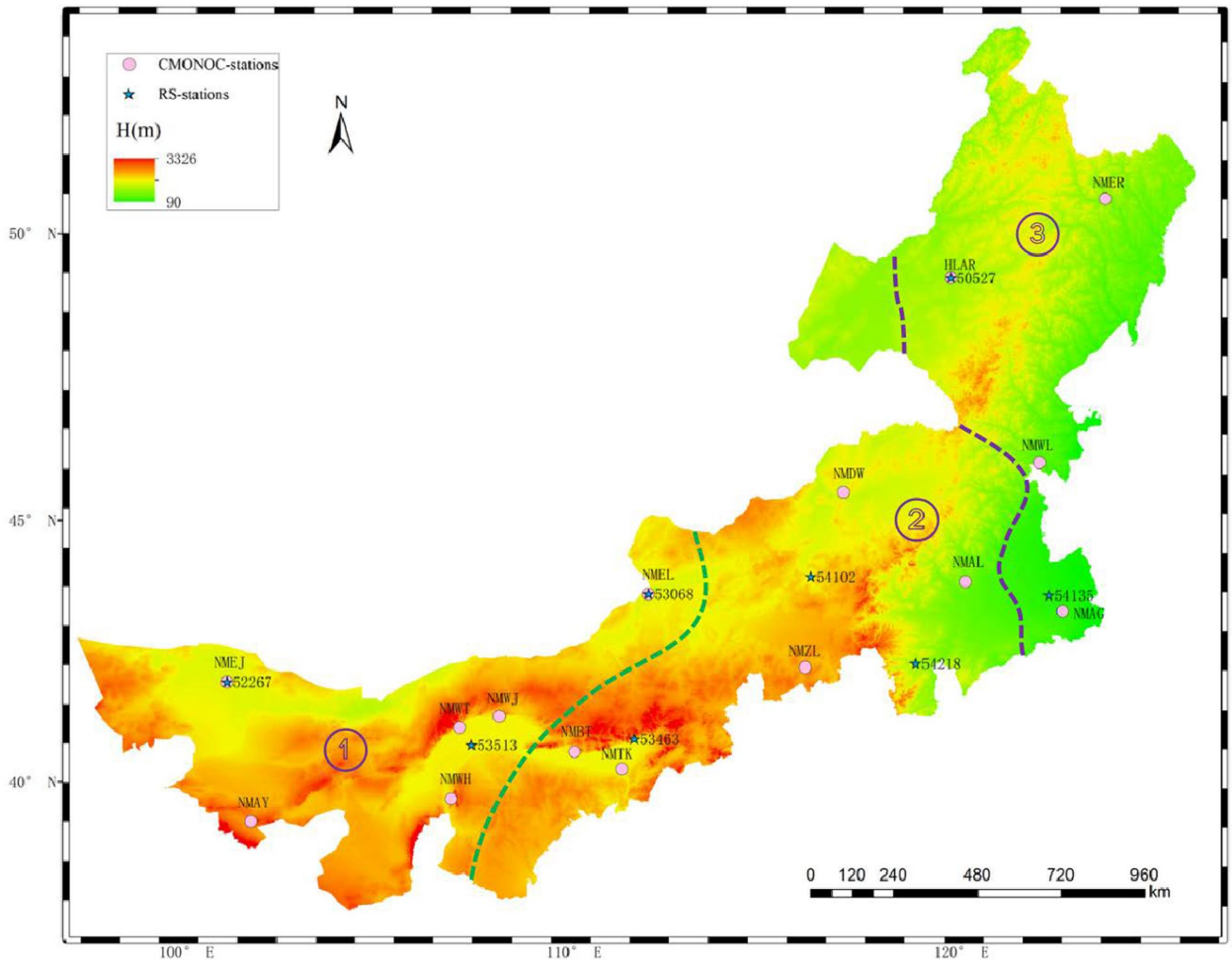

Fig. 1 Distribution map of stations in Inner Mongolia (circle: CMONOC observation stations; pentagrams: RS stations). Arid/humid zoning of Inner Mongolia with the following designations: ① arid zone, ② semi-arid zone, and ③ semi-humid zone

Table 1 Station and reanalysis data information

Datasets	Data type	Temporal resolution	Spatial/horizontal resolution	Vertical resolution	Variables	Data source
GNSS	Station data	1 h	15 stations	–	ZTD	CMONOC
RS	Station data	12 h	8 stations	–	P, T, RH, H	IGRA2
ERA5	Pressure level data	1 h	0.25° × 0.25°	37	P, T, Q, H	ECMWF
MERRA-2	Pressure level data	6 h	0.625° × 0.5°	42	P, T, Q, H	NASA

ZTD zenith total delay, *P* pressure at different levels, *T* the temperature at different levels, *RH* relative humidity, *H* geopotential height, *Q* specific humidity

of the experimental results. Each data category will be further described in the corresponding sections.

2.1.1 GNSS ZTD data

The hourly ZTD tropospheric delay products provided by CMONOC are applied to retrieve GNSS PWV. The main task of the CMONOC network with 260 GNSS stations is to monitor the crustal movements and earthquakes of China. The raw GNSS observation data were processed using GAMIT/GLOBK software for network adjustment to gain various GNSS products (Jiang et al. 2016). The observation sampling rate and cutoff angle are set to 30 s and 10°, respectively, and the final precise ephemeris, relax mode, global mapping function (GMF), and GAMIT default horizontal gradient parameters are applied to estimate the hourly ZTD (Ren et al. 2022). For this study, ZTD products from 15 CMONOC stations located in Inner Mongolia from 2019 to 2021 were used.

2.1.2 Radiosonde data

The RS observation data adopted in this research were available from the Integrated Global Radiosonde Archive Version 2 (IGRA2) dataset. The time resolution is 12 h. As independent observation data, RS data is frequently utilized to assess the accuracy of other datasets (Zhang et al. 2018a). In the Inner Mongolia region, there are eight RS stations, with three of them being co-located with the GNSS stations. In order to minimize errors due to distance and elevation differences, another 1 RS stations was chosen, which is located within 50 km and with an elevation difference of less than 200 m from the GNSS stations (Wang and Zhang 2008). Ultimately, four RS stations were applied to validate the accuracy of PWV retrieved from GNSS.

2.1.3 ERA5 data

ERA5 was released by ECMWF providing pressure-level data and single-level data since 1979; we used pressure-level data from 2019 to 2021. The horizontal resolution of the pressure-level dataset in ERA5 is 0.25° × 0.25° (longitude × latitude), the time resolution is 1 h, and the vertical part consists of 37 layers. The ERA5 dataset provides higher temporal and spatial resolution than the previous generation product ERA-Interim of ECMWF.

2.1.4 MERRA-2 data

In 1980, NASA released MERRA-2 with 6 hourly pressure-level data and hourly single-level data. The pressure-level dataset in MERRA-2 has a horizontal resolution of 0.625° × 0.5°, the time resolution of 6 h, and consists of 42 layers.

2.1.5 Methods

2.1.6 GNSS PWV retrieval method

ZTD can be categorized into zenith hydrostatic delay (ZHD) and zenith wet delay (ZWD). ZHD can be calculated by the Saastamoinen model (Saastamoinen 1972), and ZWD is achieved by stripping ZHD from ZTD. The formula for inverting PWV using GNSS observation data is (Askne and Nordius 1987):

$$\mathrm{ZHD} = \frac{0.002277 \cdot P}{1 - 0.00266 \cdot \cos(2\varphi) - 0.00000028 \cdot H}, \tag{1}$$

$$\mathrm{ZWD} = \mathrm{ZTD} - \mathrm{ZHD}, \tag{2}$$

$$\mathrm{PWV} = \Pi \cdot \mathrm{ZWD} \frac{10^6}{\rho_W R_v \left(\frac{K_3}{T_m} + K_2'\right)} \cdot \mathrm{ZWD}, \tag{3}$$

where P represents the station surface pressure (hpa); φ represents the latitude (radians); H is the station geodetic height (m); Π is water vapor conversion factor; ρ_w is the liquid water density, usually taken as $1 \times 10^3\ \mathrm{kg/m^3}$; R_v is the gas constant for water vapor, whose value is $461.495\ \mathrm{J \cdot kg^{-1} \cdot k^{-1}}$; k_2' and k_3 are atmospheric physical constants, typically taken as $22.13 \pm 2.20\ \mathrm{K/hpa}$ and $(3.739 \pm 0.012) \times 10^5\ \mathrm{K^2/hpa}$, respectively.

ZTD comes from the tropospheric products provided by CMONOC. Because of the absence of meteorological sensors on most GNSS observation stations, we utilize the high-precision meteorological parameters P by ERA5 pressure-level data to estimate ZHD. T_m represents the atmospheric weighted average temperature, gained by direct integration from ERA5.

2.1.7 PWV retrieval method with reanalysis data

For RS, ERA5, and MERRA-2, the direct integration method is employed to calculate PWV, utilizing the following formula: (Zhang et al. 2019b):

$$\mathrm{PWV} = -\frac{1}{2g} \sum_{i=1}^{n} (q_i + q_{i+1}) \cdot (p_{i+1} - p_i), \tag{4}$$

$$q = \frac{0.622e}{p - 0.378e}, \tag{5}$$

$$g(\varphi, H) = 9.80616(1 - 2.59 \times 10^{-3} \cos 2\varphi) \cdot (1 - 3.14 \times 10^{-7} H), \tag{6}$$

where i refers to the number of layers, and q_i represents the specific humidity of the i layer (hpa); p_i is the atmospheric pressure of the i layer (hpa); e denotes the water

vapor pressure (hpa); g is the acceleration of gravity, and since the values in different areas are different, this study uses the formula (6) to calculate the gravity parameters in different areas.

2.1.8 Unification of elevation system and processing method of meteorological data

To ensure accurate and reliable comparisons of the PWV calculated from different data sources, it is essential to unify the elevation data among different data sources. The ERA5 dataset is obtained from the Earth's geopotential system, and RS and MERRA-2 datasets are retrieved from the Earth's geopotential height system. However, GNSS data uses the geodetic height system. To mitigate these discrepancies, this experiment unifies different data sources under the geodetic height system. The specific method of unifying each elevation system into the geodetic height system (Wang et al. 2016) and the processing method of meteorological data are given below, the flowchart of which is shown in Fig. 2.

(1) Converting geopotential to geopotential height:

$$\mathrm{GPH} = \frac{\mathrm{GP}}{g}. \tag{7}$$

The formula GP represents the geopotential (m^2/s^2), *GPH* represents the geopotential height (m), and g represents the actual local gravity acceleration, which can be obtained from Eq. (6).

(2) Calculating orthometric height using geopotential height:

$$H'(\mathrm{GPH}, \varphi) = \frac{R(\varphi) \cdot Y_{45} \cdot \mathrm{GPH}}{Y_s(\varphi) \cdot R(\varphi) - Y_{45} \cdot \mathrm{GPH}}, \tag{8}$$

where $Y_s(\varphi)$ represents the normal gravity value on the reference ellipsoid's surface; $R(\varphi)$ refers to the effective radius of the Earth when the latitude is φ; Y_{45} represents the normal gravity value on the ellipsoid's surface at latitude 45°, with a value of 9.80665 m/s^2. The calculation formulas for $Y_s(\varphi)$ and $R(\varphi)$ are as follows:

$$Y_s(\varphi) = 9.780325 \cdot \left[\frac{1 + 0.00193185 \cdot \sin^2(\varphi)}{1 - 0.00669435 \cdot \sin^2(\varphi)}\right]^{0.5}, \tag{9}$$

$$R(\varphi) = \frac{6378137}{1.006803 - 0.006706 \cdot \sin^2(\varphi)}. \tag{10}$$

(3) Converting orthometric height to geodetic height:

$$H = H' + N, \tag{11}$$

where N represents the geoid gap usually obtained using the EGM2008 gravity model. Through the calculation of the above formula, the unification of the multi-source data elevation system can be realized.

Because of the elevation difference between the GNSS station and its adjacent four grid points, directly integrating the PWV using the grid points' elevation as the starting point would inevitably lead to accuracy loss and potentially impact the evaluation results. Therefore, to ensure the consistency in the elevation of GNSS station and the nearest four grid points, it is necessary to first perform vertical interpolation to obtain the PWV value at a site of the same elevation as those of 4 grid points around the site and then to reduce the influence of elevation inconsistency. Ultimately, horizontal interpolation is performed by the inverse distance weighting (IDW) method (Janssen et al. 2004) to obtain the PWV value of the GNSS station.

If the elevation of the target point falls within the range of the reanalysis data, the temperature and specific humidity data will be gained using linear interpolation of meteorological data between adjacent levels. The pressure data is calculated using Eqs. (12) and (13). However, if the target point's elevation is outside the range of available data, vertical extrapolation of meteorological parameters is required. For temperature, the average temperature lapse rate −6.5 K/km is typically used to estimate the value at the corresponding elevation. For the pressure and other meteorological parameters, the average parameter lapse rate can be derived applying data from the three layers closest to the elevation of the observation station, to extrapolate the estimate at the corresponding elevation (Huang et al. 2020).

$$P_H = P_{\mathrm{lower}} \cdot \exp\left(-\frac{H - H_{\mathrm{lower}}}{h_p}\right), \tag{12}$$

$$h_p = \frac{H_{\mathrm{upper}} - H_{\mathrm{lower}}}{\ln(P_{\mathrm{lower}}/P_{\mathrm{upper}})}, \tag{13}$$

where, H_{lower} represents the geopotential height of the lower layer (m), while, H_{upper} represents that of the upper layers (m); P_{lower} and P_{upper} represent the atmospheric pressure of the lower and upper layers (hpa); P_H represents the pressure when the height is H.

2.1.9 Accuracy evaluation index

Here, the correlation coefficient (R), bias, RMSE, and R-RMSE are used to assess the accuracy of the PWV

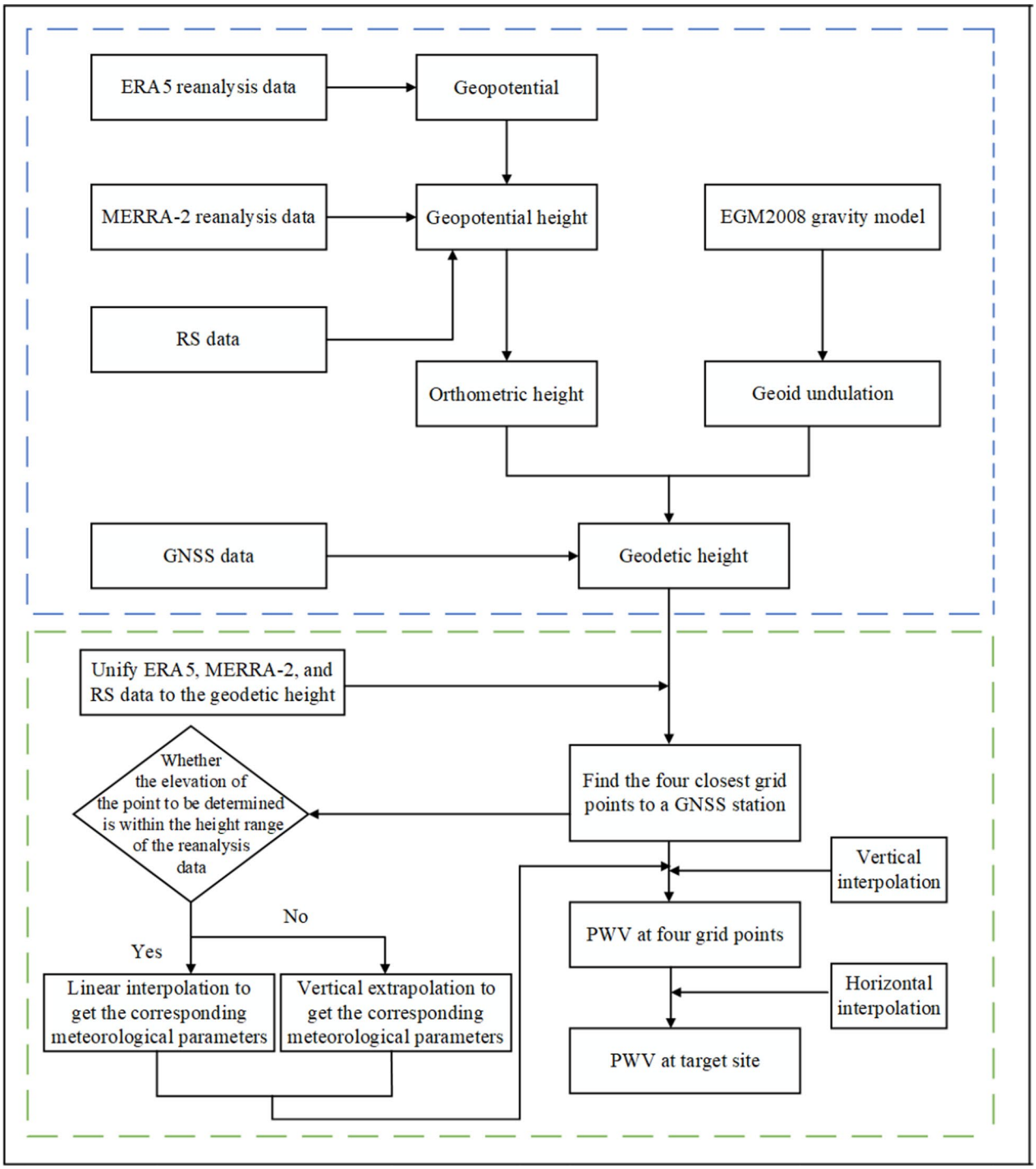

Fig. 2 Flowchart of the unification of multi-source data elevation system (above frame) and meteorological data processing method (below frame)

derived from GNSS, RS, ERA5, and MERRA-2. The expressions are shown below:

$$R = \frac{\sum_{i=1}^{n}\left(Y_i - \overline{Y_i}\right)\cdot\left(Y_i - \overline{Y_i'}\right)}{\sqrt{\sum_{i=1}^{n}\left(Y_i - \overline{Y_i}\right)^2 \cdot \sum_{i=1}^{n}\left(Y_i - \overline{Y_i'}\right)^2}}, \tag{14}$$

$$\text{Bias} = \frac{\sum_{i=1}^{n}(Y_i - Y_i')}{n}, \tag{15}$$

$$\text{RMSE} = \sqrt{\frac{\sum_{i=1}^{n}(Y_i - Y_i')^2}{n}}, \tag{16}$$

$$R - \text{RMSE} = \sqrt{\frac{\text{RMSE}}{\overline{Y_{\text{i}}'}}}, \tag{17}$$

where Y_i and $\overline{Y_i}$ represent the calculated value of the parameter to be evaluated and its average value, respectively; Y_i' and $\overline{Y_i'}$ represent the reference value of the test and its average value, respectively; n represents the number of samples.

2.1.10 Gross error detection of PWV time series

To guarantee the reliability of the experimental results, outlier detection and quality control on the PWV time series should be performed to eliminate the influence of gross errors. In this study, to enhance the robustness of gross error detection, the interquartile range (IQR) criterion is applied to get rid of gross errors under the assumption that the detected target sequences follow a standard normal distribution. Suppose that when the target series is sorted in ascending order, the 25th percentile represents the lower quartile, and the 75th percentile refers to the upper quartile. IQR is obtained by taking the difference between the upper quartile and the lower quartile, and the IQR-based outlier detection interval is defined as follows (Xu et al. 2022):

$$\text{IQR} = Q3 - Q1, \tag{18}$$

$$[Q1 - 1.5\cdot\text{IQR}, Q3 + 1.5\cdot\text{IQR}], \tag{19}$$

where $Q1$ represents the lower quartile, and $Q3$ refers to the upper quartile. By formula (19), the values outside this range are marked as outliers and removed to ensure the reliability of the evaluation results.

3 Results and analysis

3.1 Evaluation and comparison of the Tm model

Tm is a key factor in the GNSS PWV inversion process, and selecting a Tm model with higher accuracy can effectively improve the accuracy of GNSS PWV. There are many commonly used Tm models, such as the classic Bevis model (Bevis et al. 1992) and the widely used global pressure and temperature (GPT) model (Landskron and Böhm 2018), as well as the direct integration of meteorological reanalysis data ERA5 and MERRA-2 to obtain Tm. The Bevis model requires the provision of measured surface temperature to obtain Tm, and research has shown that the Bevis model performs well in accuracy in mid- to high-latitude areas (Yu and Liu 2009; Xu et al. 2022). GPT3 is the latest non-measured meteorological parameter tropospheric delay estimation model in the GPT series, with horizontal resolutions of 1° × 1° (GPT3-1) and 5° × 5° (GPT3-5), and can provide various tropospheric parameters including Tm. To improve the reliability of GNSS PWV and reduce Tm calculation errors, this paper uses the Tm obtained from RS station integration from 2019 to 2021 as a reference value to evaluate the accuracy of Tm obtained from the Bevis model, GPT3-1 model, MERRA-2, and ERA5 integration in Inner Mongolia. The bias and RMSE statistical results of the four models are shown in Table 2.

From Table 2, it can be seen that compared to other models, the bias and RMSE of the Bevis model are both the highest, at 4.88 and 5.83 K, respectively. The accuracy of Tm obtained by MERRA-2 integration is better than that of the GPT3-1 model, but the accuracy improvement is limited. The accuracy of Tm obtained by ERA5 integration is the highest, with bias and RMSE of 0.76 and 3.00 K, respectively. Therefore, this paper chooses the Tm obtained by ERA5 integration for subsequent GNSS PWV inversion.

According to Eq. (3), Tm is a key factor affecting PWV. To study the impact of Tm on GNSS PWV, the error propagation law is used to estimate the uncertainty of GNSS inverted PWV, as follows (Namaoui et al. 2017):

$$\sigma_{\text{PWV}}^2 = \left[10^6 \text{ZWDR}_v \frac{K_3}{(R_v K_3 + R_v K_2' T_m)^2}\right]\sigma_{T_m}^2, \tag{20}$$

Table 2 The bias and RMSE statistical results of different models

Models	bias (K)	RMSE (K)
Bevis	4.88	5.83
GPT3-1	−1.85	5.71
MERRA-2	−1.68	5.34
ERA5	0.76	3.00

where, σ_{PWV} and σ_{Tm}, respectively, represent the errors of PWV and Tm.

Through calculation, it can be seen that the impact of Tm deviation on GNSS PWV varies among different stations. Among them, the NMAG station has the greatest impact of Tm deviation on GNSS PWV: σ_{PWV} is 2.01 mm; the NMEJ station has the least impact: σ_{PWV} is 1.35 mm; The average of 15 stations σ_{PWV} is 1.64 mm. The results indicate that the uncertainty of Tm values resulted in a small difference of no more than 2 mm in the final estimation of GNSS PWV.

3.2 Comparison between RS PWV and GNSS PWV

PWV estimated by RS is often used as a metric to assess other atmospheric reanalysis products. Accuracy verification is necessary before GNSS PWV is used to assess other reanalysis data. Due to poor data quality and severe data missing at the NMWT station, this site is not considered. Therefore, to validate the reliability of GNSS PWV in the Inner Mongolia region, a study was conducted using the RS PWV data from four RS stations described in Sect. 2.1.2. The time series changes of PWV for RS and GNSS from 2019 to 2021 are shown in Fig. 3, and the correlation analysis is shown in Fig. 4. During the comparison process, quality control was implemented to the PWV time series.

From Fig. 3, it can be seen that the time series of the two exhibit obvious annual, semi-annual, and seasonal variations, and have the same trend of change. Due to the missing RS data in the second half of 2021, only the changes in GNSS PWV are displayed. Figure 4 demonstrates a strong correlation and good agreement between the PWV retrieved from GNSS and RS, with correlation coefficients consistently above 0.9. Those results show that in Inner Mongolia, the PWV retrieved by GNSS can be used as a reference value to assess the PWV accuracy of the ERA5 and MERRA-2 datasets. This study conducted a comparative analysis of PWV derived from GNSS and RS data on four stations in Inner Mongolia. The comparison involved analyzing the bias and RMSE of these two kinds of PWV, which are shown in Fig. 5.

According to Fig. 5, we know that the average bias range of PWV between GNSS and RS for the four stations is from −0.92 to −0.18 mm, and the RMSE range is from 1.86 to 2.73 mm. The overall average bias and RMSE for four stations are −0.68 and 2.17 mm, respectively. It can be observed that the bias of all four stations is less than 1 mm, and the RMSE is less than 3mm. The bias values of all four stations are negative, indicating that the PWV derived from GNSS data are slightly lower than those derived from RS. The negative bias of the four stations can be attributed to the different detection technologies of RS and GNSS (Huang et al. 2021b). GNSS PWV has shown high accuracy and good applicability, which is about equal to the accuracy of PWV of the previous studies (Zhao et al. 2019). Therefore, these findings further support that the PWV obtained from GNSS can be looked as the reference for evaluating PWV values derived from other reanalysis data.

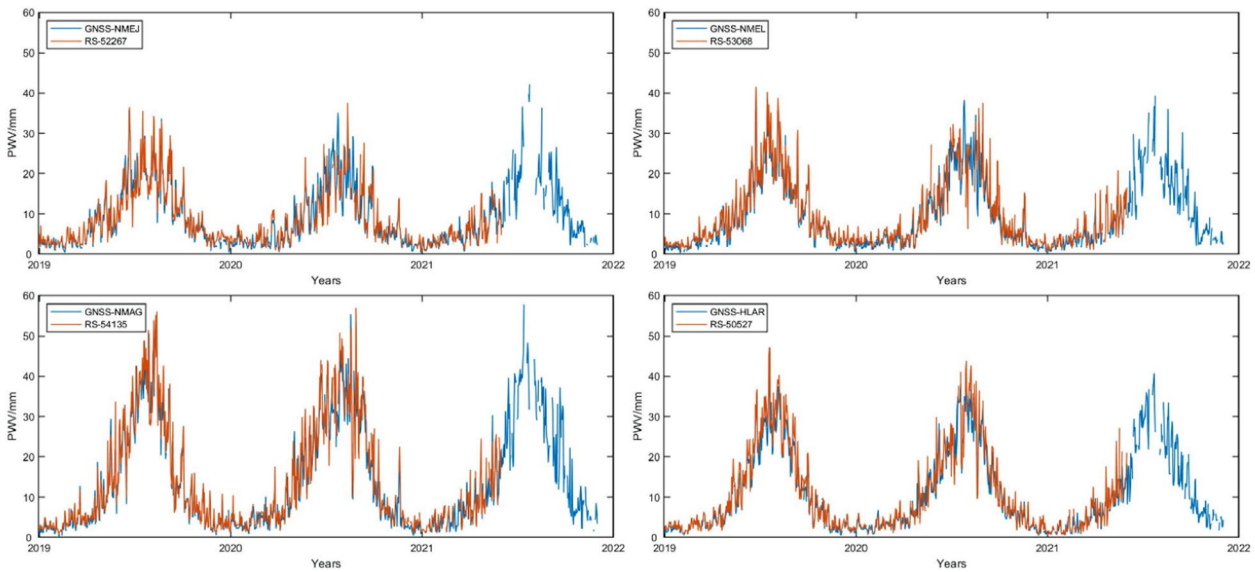

Fig. 3 Time series changes of RS PWV and GNSS PWV in Inner Mongolia from 2019 to 2021

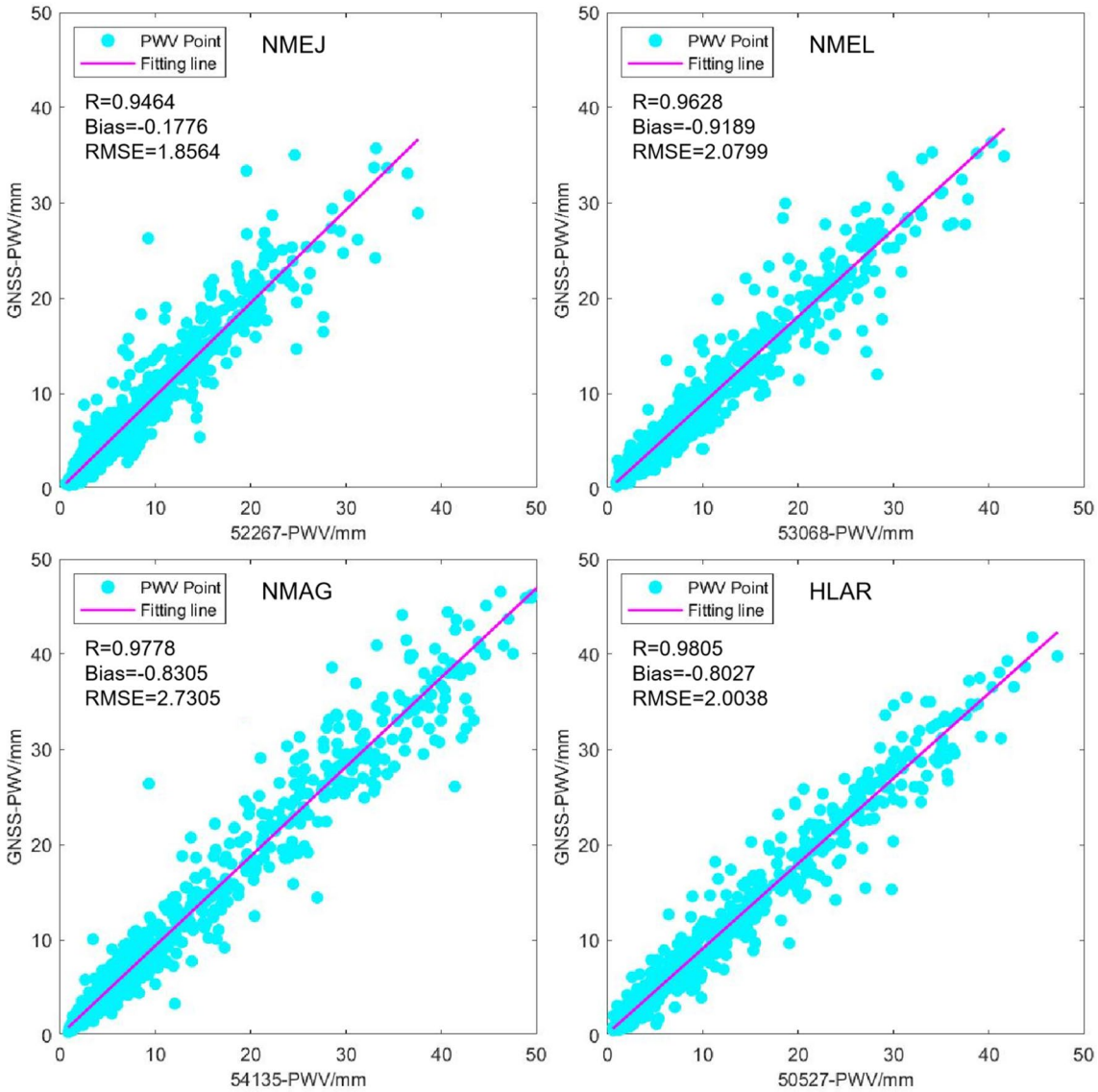

Fig. 4 Correlation analysis between PWV of GNSS and RS in 2019–2021

3.3 Analysis of PWV retrieved from GNSS, ERA5, and MERRA-2

3.3.1 Analysis of PWV annual variation

Before comparing the annual changes of PWV, two stations were selected from arid, semi-arid, and semi humid regions for correlation analysis between GNSS PWV, ERA5 PWV, and MERRA-2 PWV, as shown in Figs. 6 and 7. The PWVs retrieved from 15 GNSS stations in Inner Mongolia from 2019 to 2021 were used as reference values and compared with the PWVs obtained from ERA5 and MERRA-2 inversion. Figures 8 and 9, respectively, show the annual average deviation and RMSE distribution of PWV relative to GNSS for ERA5 and MERRA-2. The evaluation results for different arid and humid zones in Inner Mongolia are displayed in Table 3.

From Figs. 6 and 7, it can be seen that ERA5 PWV and MERRA-2 PWV have a strong correlation with GNSS PWV, especially ERA5 PWV, whose correlation with GNSS PWV is above 0.99, indicating a higher consistency between GNSS PWV and ERA5 PWV. This is mainly due to ERA5 assimilating a large amount of remote sensing satellite observation data and adopting advanced data assimilation methods, thereby improving the inversion accuracy of PWV. In addition, its high spatiotemporal resolution enables ERA5 to more accurately capture the details of atmospheric

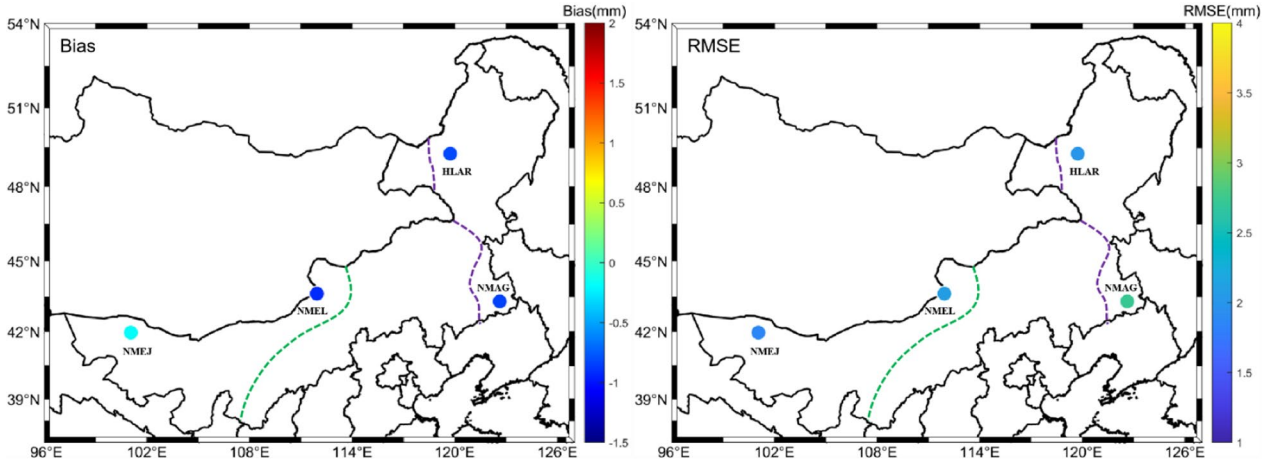

Fig. 5 The time series bias (left) and RMSE (right) distributions at the four selected stations from 2019 to 2021

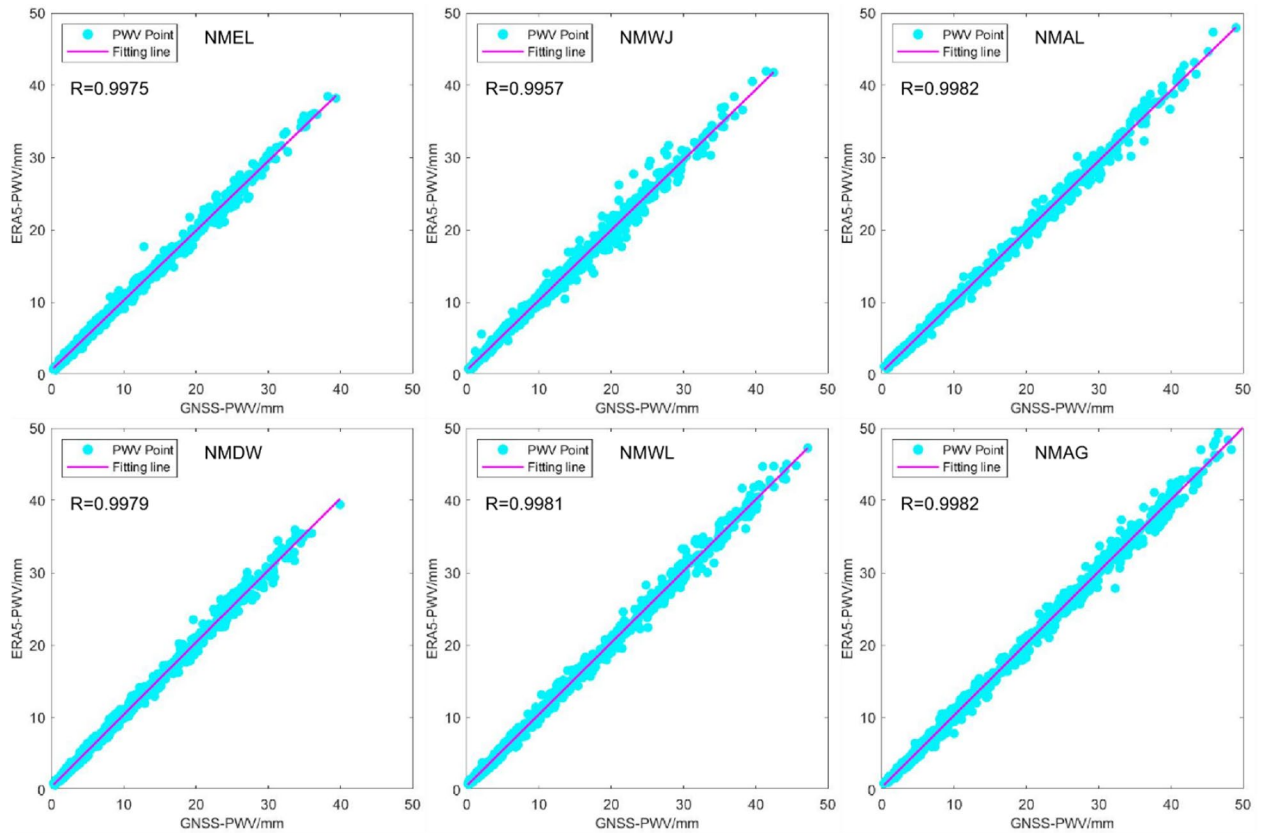

Fig. 6 Correlation analysis between PWV of GNSS and ERA5 in 2019–2021

phenomena (Wang 2021; Huang et al. 2022b). Figure 8 indicates that ERA5 PWV exhibits a smaller annual average bias compared to MERRA-2 PWV, indicating a higher accuracy for ERA5 PWV. Additionally, ERA5 PWV shows more positive bias in the Inner Mongolia region, suggesting that GNSS PWV are smaller than ERA5 PWV values. The ranges of PWV bias retrieved by ERA5 and MERRA-2 are from −0.15–0.54 mm and −1.33–1.93 mm, and the overall annual average bias is 0.17 and 0.39 mm, respectively. Overall, ERA5 PWV exhibits slightly higher accuracy than MERRA-2. In Fig. 9, the annual average RMSE for both reanalysis

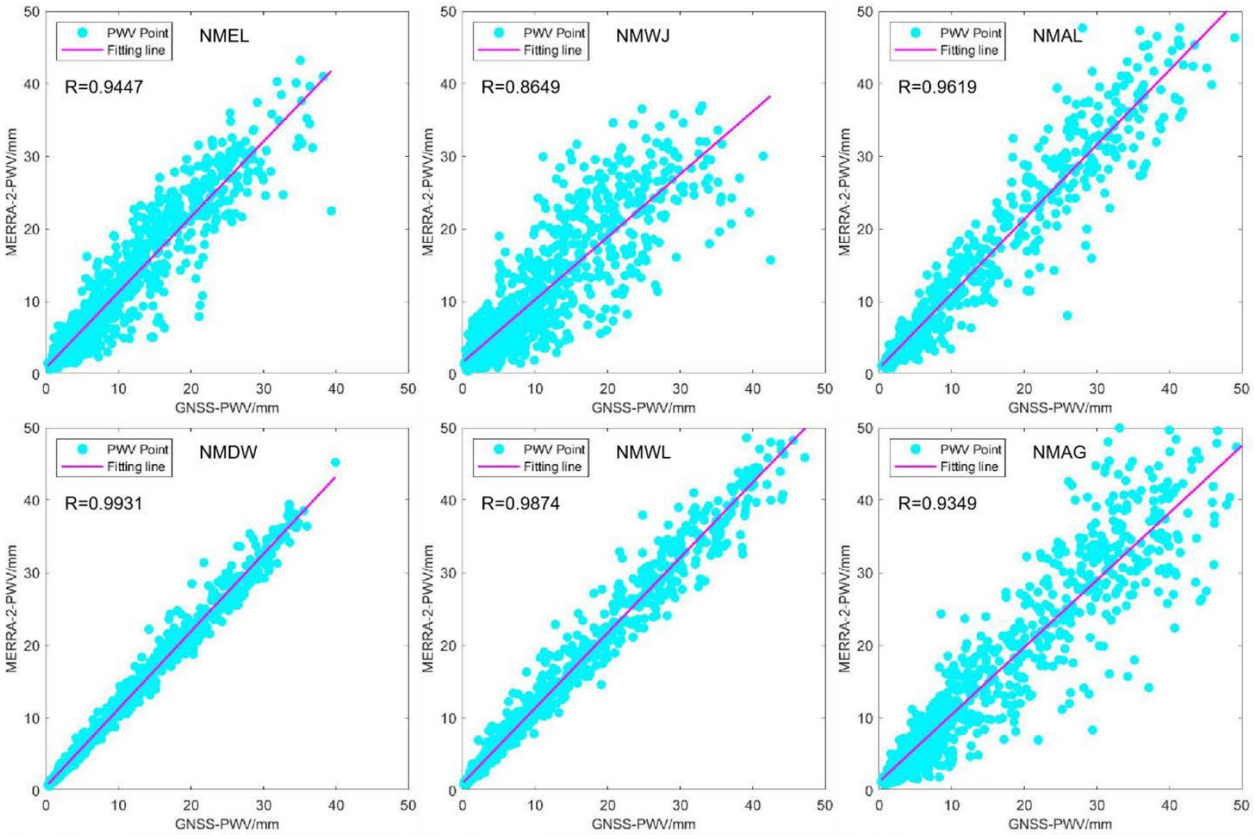

Fig. 7 Correlation analysis between PWV of GNSS and MERRA-2 in 2019–2021

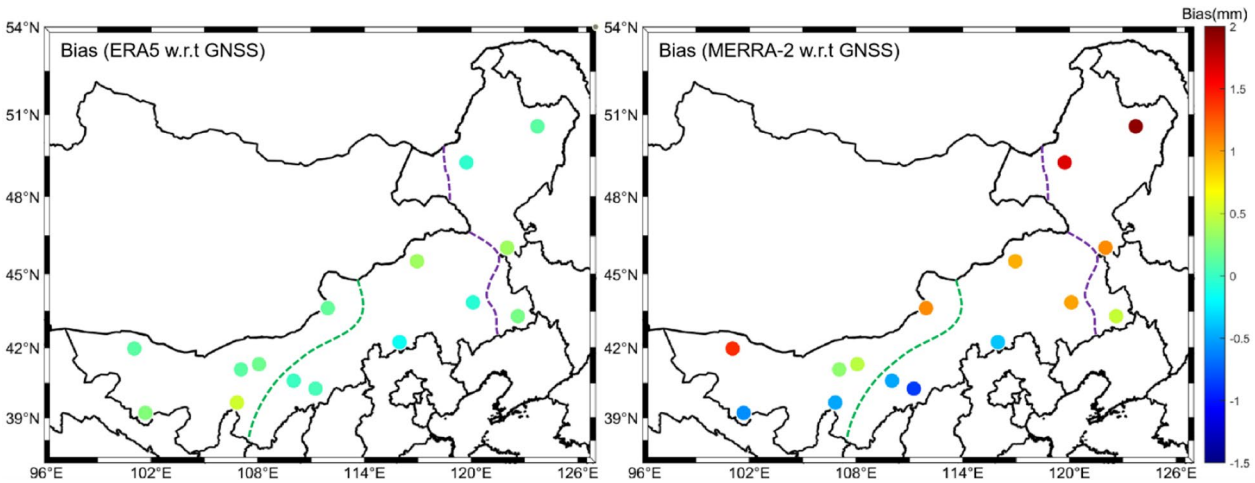

Fig. 8 The annual average bias distribution of PWV of ERA5 (left) and MERRA-2 (right) relative to that of GNSS in the Inner Mongolia region from 2019 to 2021

datasets exhibits similar distribution characteristics to bias. The RMSE ranges for ERA5 PWV and MERRA-2 PWV are 1.33–2.00 mm and 1.83–3.82 mm, respectively, and overall annual average RMSEs are 1.63 and 2.99 mm, respectively. The above analysis indicates that the accuracy of PWV from ERA5 is significantly higher than that from MERRA-2. The reason may be that the spatial and temporal resolution of ERA5 reanalysis data is better than that of MERRA-2, and the distribution of MERRA-2 PWV at individual stations (NMER) in

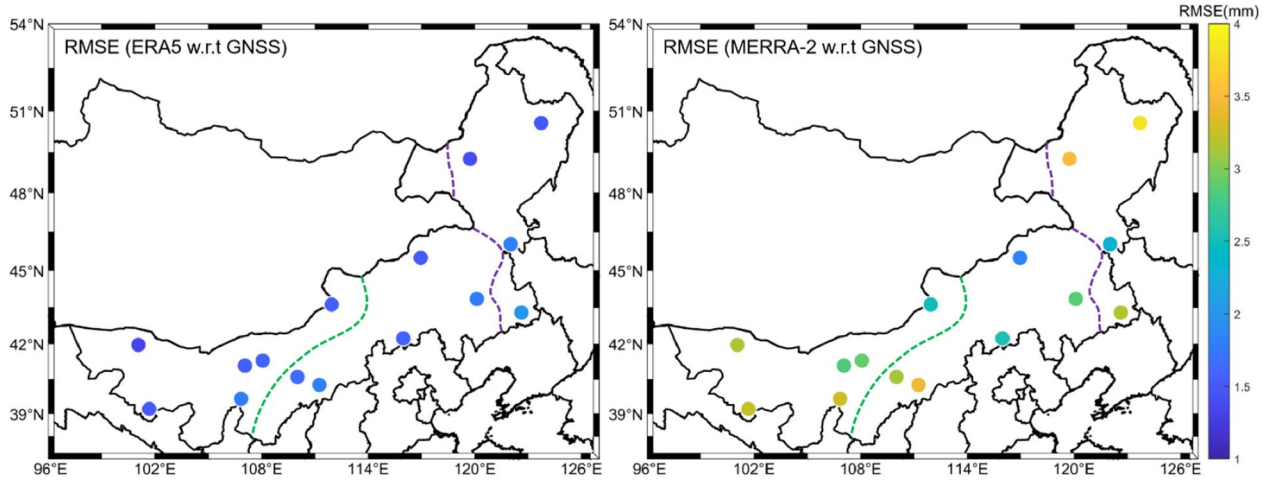

Fig. 9 The annual average RMSE distribution of PWV of ERA5 (left) and MERRA-2 (right) relative to that of GNSS in the Inner Mongolia region from 2019 to 2021

Table 3 Statistics of PWV from ERA5 and MERRA-2 relative to that from GNSS in 2019–2021 (mm)

Reanalysis data	Arid zone			Semi-arid zone			Semi-humid zone			Inner Mongolia region		
	Bias	RMSE	R-RMSE (%)	Bias	RMSE	R-RMSE (%)	Bias	RMSE	R-RMSE (%)	Bias	RMSE	R-RMSE (%)
ERA5	0.29	1.57	20.90	0.07	1.65	18.86	0.17	1.68	18.14	0.17	1.63	19.57
MERRA-2	0.12	3.03	36.12	0.04	2.76	37.87	1.59	3.20	32.75	0.39	2.99	35.83

the semi-humid zone shows significant errors, with an RMSE of 3.82 mm. This could be attributed to factors such as higher precipitation and higher water vapor content in the semi-humid zone compared to other zones in Inner Mongolia.

According to the statistics in Table 3, for ERA5 PWV, the largest bias occurs in the arid zones with a value of 0.29 mm, while the smallest bias appears in the semi-arid zones with a value of 0.07 mm. The maximum and minimum bias of MERRA-2 PWV appear in the semi-humid and the semi-arid zones, respectively, with values of 1.59 and 0.04 mm. The maximum RMSE values for both reanalysis datasets occur in the semi-humid zones, with values of 1.68 mm for ERA5 PWV and 3.20 mm for MERRA-2 PWV; the smallest R-RMSE occurs in the semi-humid zone, with rates of 18.14 and 32.75%, respectively, and an average annual R-RMSE of 19.57 and 35.83%, respectively. Overall, the average annual bias and RMSE in semi-humid zones are relatively big, which may be related to the higher precipitation and more drastic changes in water vapor in semi-humid zones compared with the other two zones. In the abundant water vapor of the semi-humid zones of Inner Mongolia, the Greater Khingan Mountains play a crucial role. In summer, warm and humid air from the Pacific flows northward, and when it climbs along the mountains, it becomes cold and forms rainfall, resulting in annual precipitation of over 400 mm in the semi-humid zones east of the mountains.

The above test proved that the accuracy of ERA5 PWV in Inner Mongolia is superior to that of MERRA-2 PWV, and it shows better consistency with GNSS PWV. Therefore, when studying interannual variations of GNSS PWV, it is recommended to use the ERA5 dataset to fill in the missing values in the PWV time series.

3.3.2 Analysis of PWV monthly variation

The goal of this paper is to study water vapor variations in different zones with distinct drought and humidity conditions utilizing PWV of GNSS, ERA5, and MERRA-2 on a temporal scale. To achieve this, monthly average PWV data from six GNSS stations in Inner Mongolia from 2019 to 2021 were used, as shown in Fig. 10. From Fig. 10, we can see that the monthly average PWV retrieved from the ERA5 and MERRA-2 datasets is in good agreement with the PWV retrieved from GNSS, and shows obvious seasonal changes. PWV reaches its peak during the

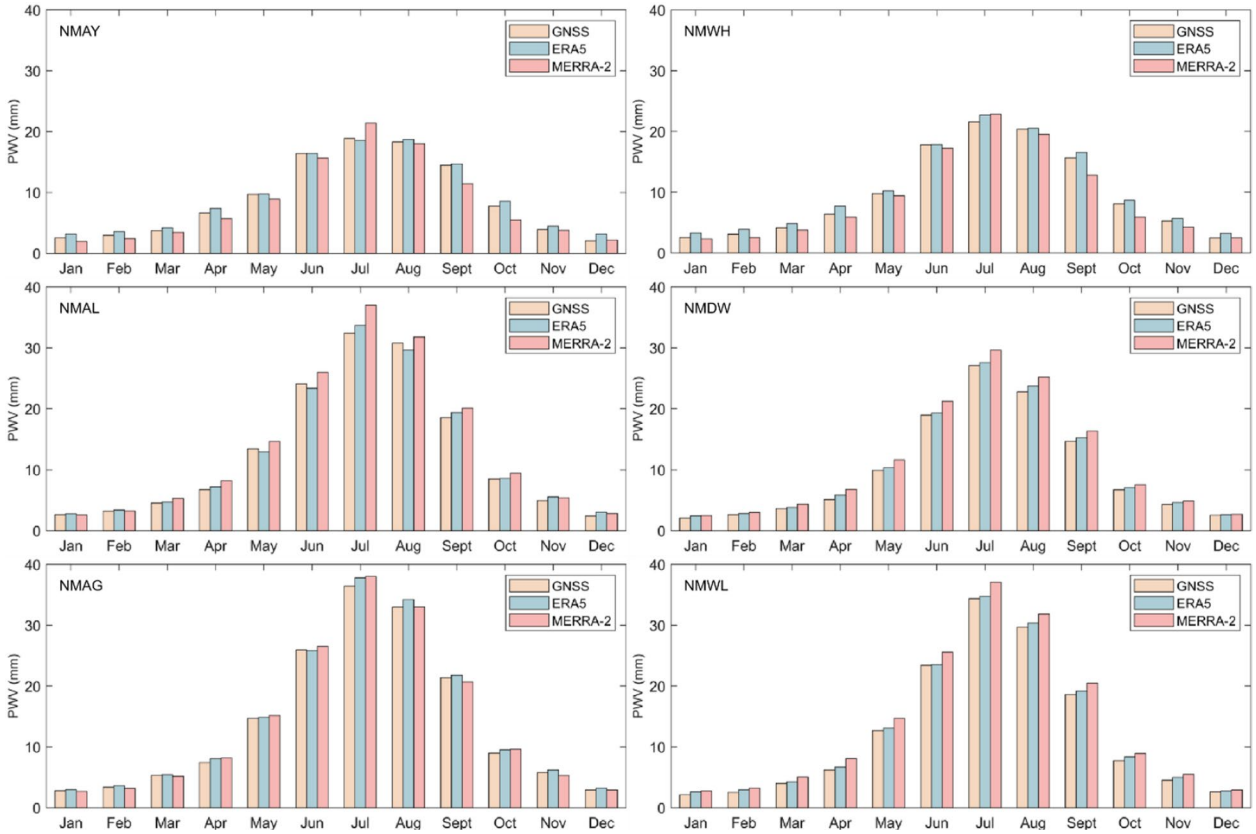

Fig. 10 The monthly average PWV retrieved by GNSS, ERA5, and MERRA-2 from 2019 to 2021 at six GNSS stations (the upper picture is the arid area, the middle picture is the semi-arid area, and the lower picture is the semi-humid area)

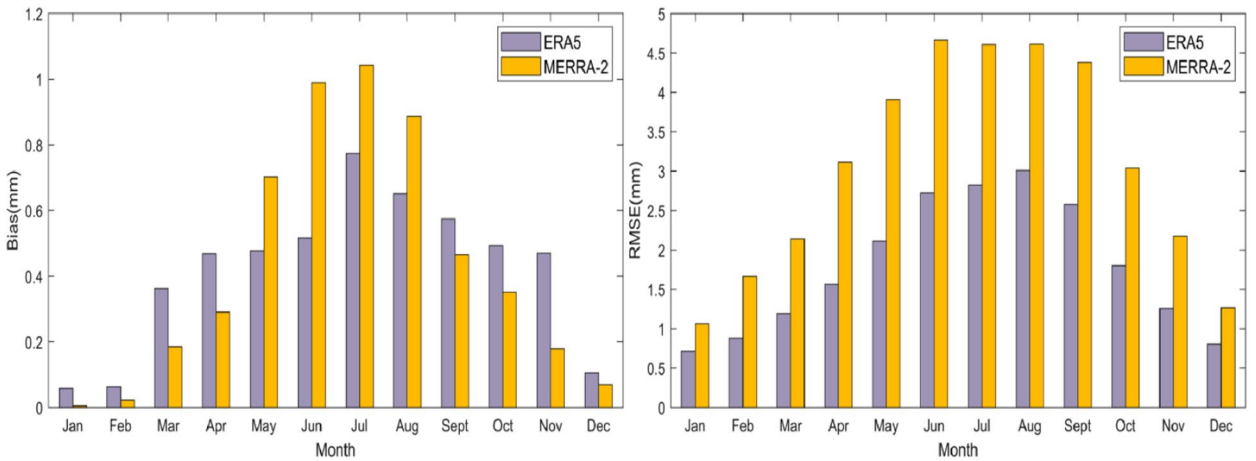

Fig. 11 Monthly average bias (left) and RMSE (right) of ERA5 PWV and MERRA-2 PWV relative to GNSS PWV in 2019–2021

summer and reaches its lowest point during the winter. This is primarily attributed to higher precipitation levels during summer compared to other seasons, leading to significant fluctuations in water vapor.

Furthermore, due to the unique geographical location of Inner Mongolia, there are significant differences in PWV between different zones. In the arid zone, the monthly average PWV generally does not exceed 25 mm,

while in the semi-arid zone, PWV can reach a maximum of 35 mm. In the semi-humid zone, due to higher precipitation compared to other zones, PWV can reach about 40 mm.

Figure 11 displays the monthly average bias and RMSE of PWV from ERA5 and MERRA-2 relative to that from GNSS of 15 GNSS stations in Inner Mongolia. Both bias and RMSE display noticeable seasonal variations. The monthly average bias of PWV retrieved by the two datasets are 0.41 and 0.43 mm, respectively. In terms of monthly average RMSE, ERA5 PWV demonstrates significantly higher accuracy than MERRA-2 PWV throughout the year, with corresponding RMSE values of 1.79 and 3.05 mm, respectively. Overall, GNSS, ERA5, and MERRA-2 provide PWV data with comparable accuracy, effectively capturing monthly average variations. However, MERRA-2 PWV is more sensitive to seasonal variations, while ERA5 PWV is less affected by these variations. From a temporal perspective, seasonal variations are the primary factors influencing PWV accuracy.

3.3.3 Analysis of PWV diurnal variation

In the investigation of the diurnal variation of PWV, GNSS PWV presents distinct advantages with high temporal resolution and accuracy. On the other hand, PWV inverted from reanalysis data holds tremendous potential because of its high spatial resolution (Zhang et al. 2021). To facilitate comparison, 1 h time resolution of MERRA-2 reanalysis data was achieved by the linear interpolation method. To assess the reliability of PWV diurnal variations represented by the two reanalysis datasets, the daily average PWV was subtracted from the corresponding PWV observations at each time point to obtain the hourly PWV diurnal anomaly variation. Additionally, to verify the influence of the different arid/humid zones in Inner Mongolia on diurnal anomaly variations, we selected 9 relatively evenly distributed sites from the 15 GNSS stations to study the daily anomaly variation time series from 2019 to 2021, as shown as in Fig. 12.

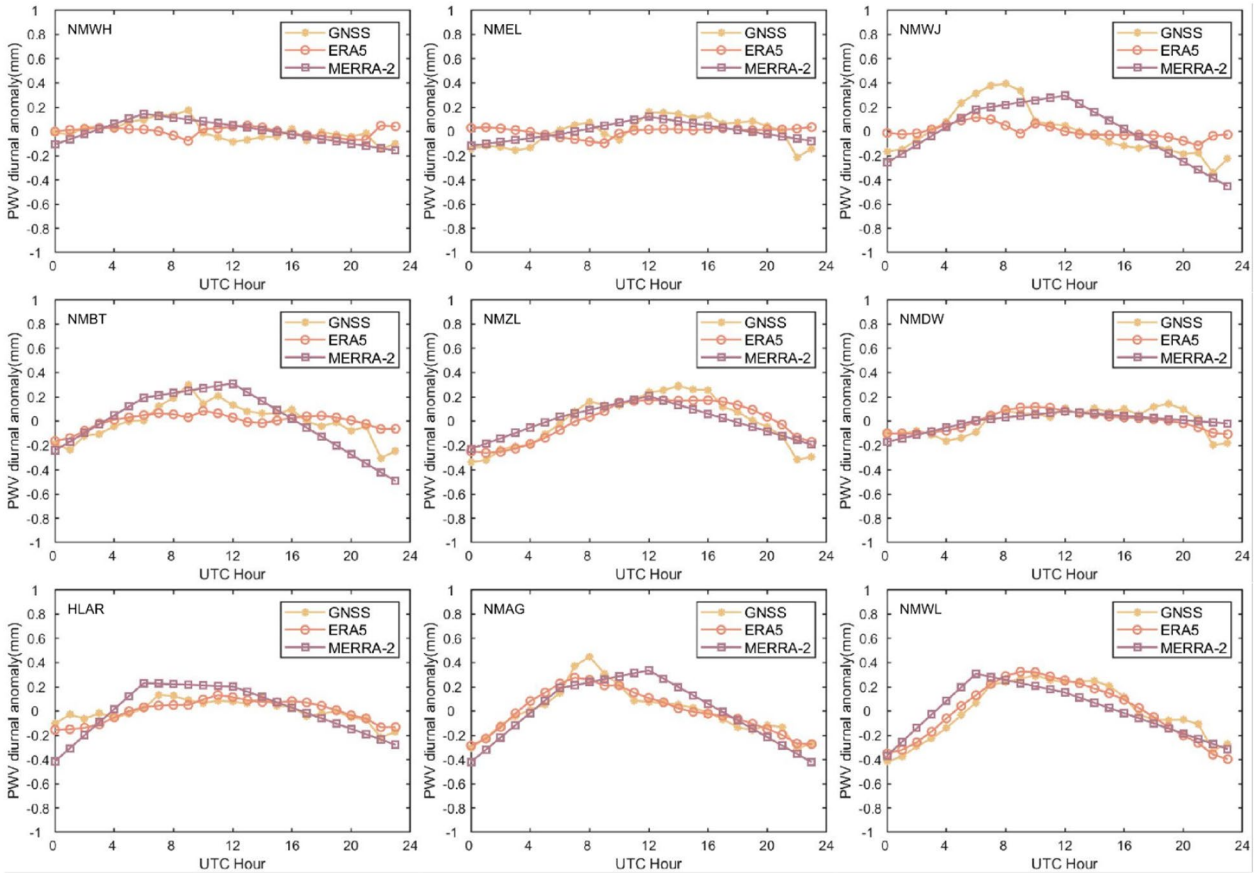

Fig. 12 Estimated diurnal variation of PWV in Inner Mongolia based on GNSS, ERA5, and MERRA-2 (the upper picture is the arid area, the middle picture is the semi-arid area, and the lower picture is the semi-humid area)

From Fig. 12, we can observe that the average diurnal anomaly of PWV for the three datasets exhibits similar overall trends at different stations, demonstrating good consistency among them. The diurnal anomaly values at the stations located in the arid zone show the smallest range of variation, remaining within ±0.3 mm. The stations in the semi-arid zone exhibit diurnal anomaly variations within ±0.4 mm, with the NMDW station showing the best consistency among the three datasets, fluctuating within ±0.2 mm. The stations in the semi-humid zone display relatively larger diurnal anomaly variations and fluctuations. The PWV exhibits distinct diurnal variation characteristics, with the diurnal anomaly values within ±0.6 mm.

The above test results may be attributed to the influence of the geographical position of Inner Mongolia, the distribution of precipitation follows a pattern of decreasing precipitation from east to west. The arid zone, located farthest from the Pacific Ocean, is least affected by maritime influences. It is also characterized by mountain barriers, such as the Yin Mountains running from east to west, numerous deserts, and relatively low and stable water vapor content. Furthermore, the semi-humid zone is closer to the ocean and is influenced by maritime monsoons. The vast forests of the Greater Khingan Mountains can transport moisture from the ocean, providing relatively abundant water vapor. Consequently, the semi-humid zone exhibits greater fluctuations in water vapor content, leading to larger diurnal anomaly variations at stations located within this zone. Furthermore, ERA5 PWV exhibits significantly higher consistency in both diurnal anomaly amplitude and phase aspects with GNSS PWV. At certain stations, significant differences exist between PWV of GNSS and ERA5, such as the NMWJ station in the arid zone, but they still clearly reflect the diurnal variation characteristics. This could be due to the relatively lower spatiotemporal resolution of the MERRA-2 dataset and the inevitable decrease in its accuracy caused by data interpolation. Therefore, it once again shows that the PWV retrieved by ERA5 is more appropriate for studying the diurnal anomaly variation in Inner Mongolia.

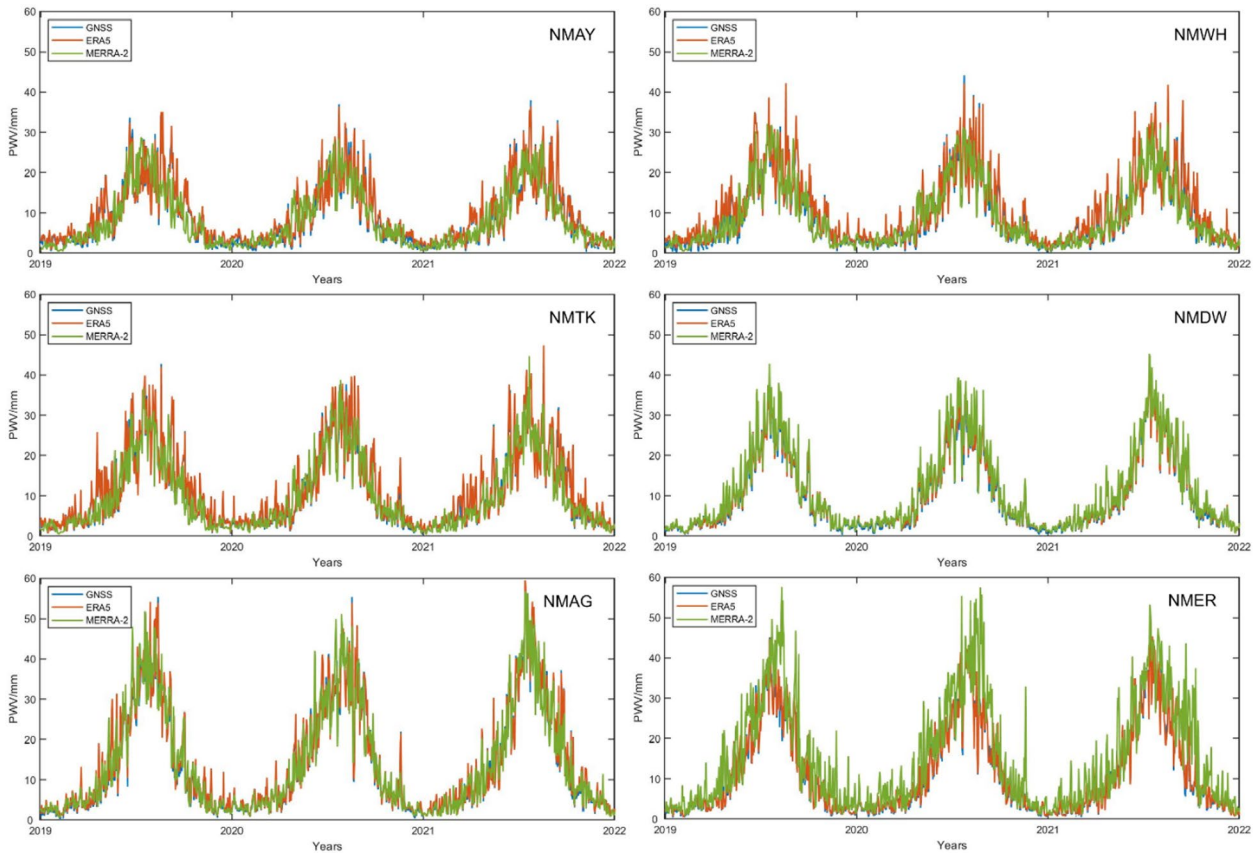

Fig. 13 Time series changes of GNSS, ERA5, and MERRA-2 PWV in Inner Mongolia from 2019 to 2021 (the upper picture is the arid area, the middle picture is the semi-arid area, and the lower picture is the semi-humid area)

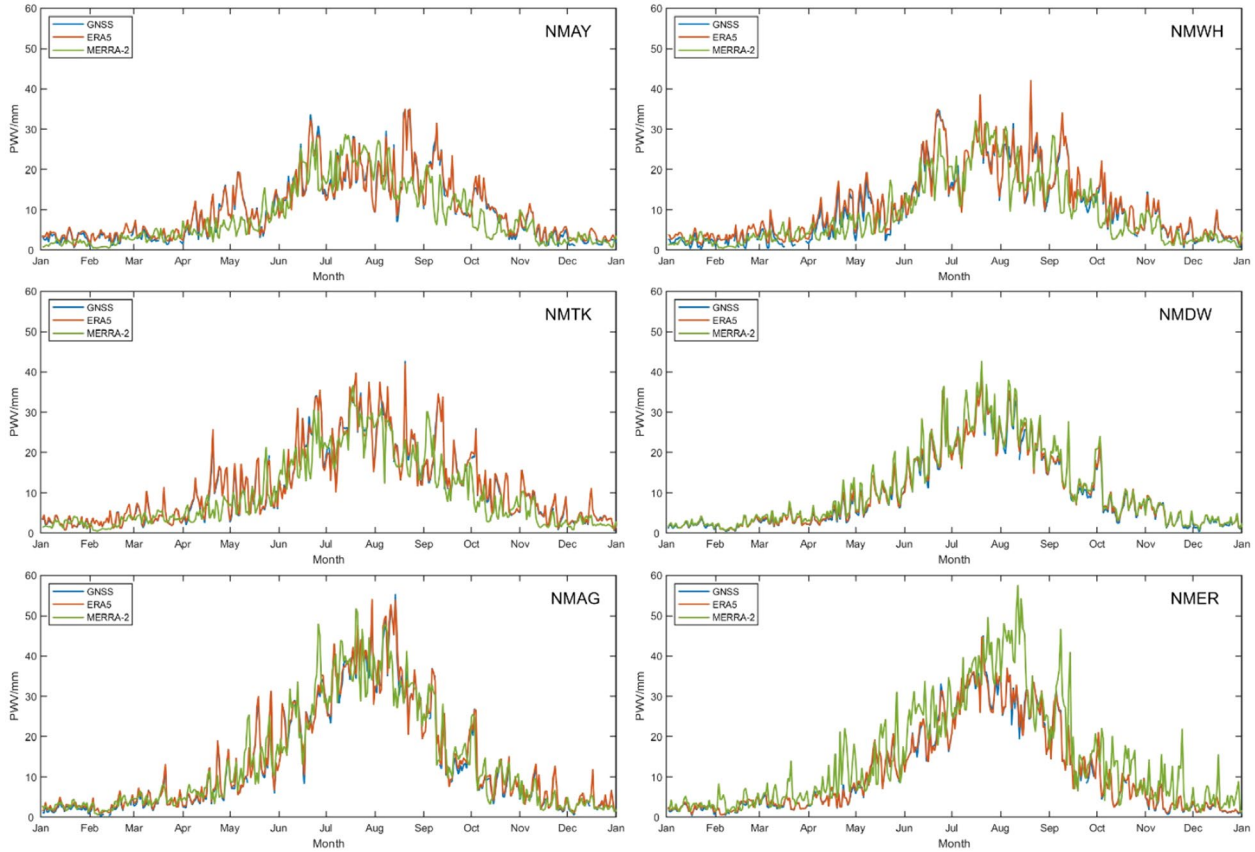

Fig. 14 Monthly changes of GNSS, ERA5, and MERRA-2 PWV in Inner Mongolia in 2019 (the upper picture is the arid area, the middle picture is the semi-arid area, and the lower picture is the semi-humid area)

3.4 Analysis of the spatiotemporal distribution characteristics of PWV

3.4.1 Analysis of PWV temporal changes

To explore the factors that affect the accuracy of PWV inversion from reanalysis data, this section analyzes the PWV obtained from reanalysis data from a temporal perspective. Two stations were selected from arid, semi-arid, and semi-humid regions, and the time series changes of the three datasets are shown in Fig. 13. From the figure, it can be seen that the PWV time series exhibits characteristics such as annual, semi-annual, and seasonal cycles. Compared with MERRA-2 PWV, the trend

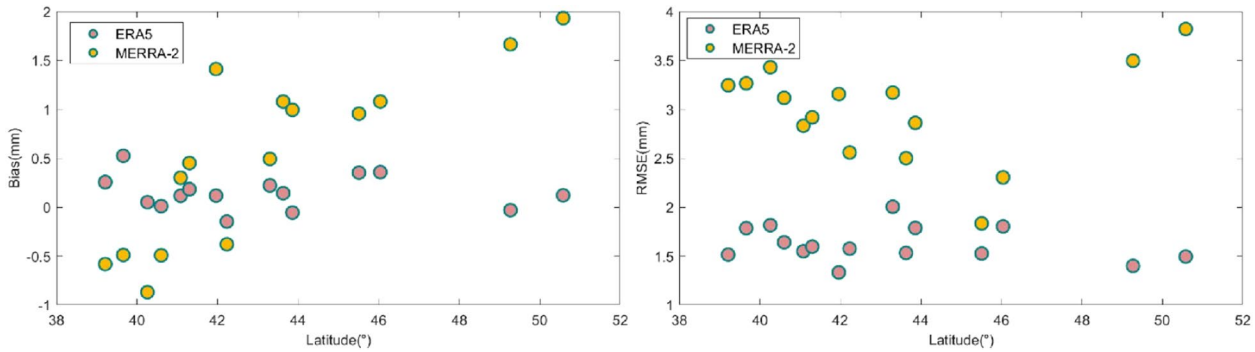

Fig. 15 The variation of annual average bias (left) and RMSE (right) of ERA5 and MERRA-2 PWV relative to GNSS PWV with latitude for all stations in Inner Mongolia from 2019 to 2021

of ERA5 PWV and GNSS PWV is more consistent. At the same time, it can be seen that PWV changes significantly from arid to semi-humid areas, with PWV maintained within 30 mm in arid areas and 40 mm in semi-arid areas, and PWV reaching a maximum of around 60 mm in semi humid areas. Figure 14 shows the monthly changes of GNSS, ERA5, and MERRA-2 PWV in Inner Mongolia in 2019. The figure indicates that PWV exhibits significant seasonal variation, reaching its peak in summer and the smallest in winter, exhibiting the same characteristics in both dry and wet zones.

3.4.2 Analysis of PWV spatial variation

Figure 15 illustrates the variation of the annual average bias and RMSE of ERA5 and MERRA-2 PWV relative to GNSS PWV with latitude for all stations in Inner Mongolia from 2019 to 2021. The abscissa indicates that the stations are arranged in the order from low latitude to high latitude. It can be observed that the PWV estimated by the two reanalysis datasets exhibits a certain correlation with latitude. The bias and RMSE of ERA5 show relatively little variation with latitude, while the bias of MERRA-2 shows an overall upward trend with increasing latitude. The RMSE value displays a decreasing trend with the increase in latitude, indicating an improvement in accuracy with the increase of latitude. However, the situation is exactly the opposite for two stations (HLAR and NMER). This could be due to both stations being in semi-humid zone and seriously influenced by the Greater Khingan Mountains, where precipitation is relatively abundant, resulting in more significant variations in atmospheric water vapor content and lower PWV accuracy. Furthermore, from Fig. 15, it can be observed that ERA5 has a smaller RMSE compared to MERRA-2, indicating better agreement with GNSS PWV.

Figure 16 illustrates the annual average bias and RMSE changes of each station with elevation from 2019 to 2021. The abscissa indicates that the elevation of each station is arranged in order from low to high. From Fig. 16, it can be observed that similar to the latitude variation, the ERA5 bias and RMSE show little variation with elevation. The bias and RMSE of MERRA-2 exhibit a decreasing trend with the increasing station elevation. This is mainly because at higher elevations, the range of PWV variation is relatively narrow, and these high-elevation stations are located in the arid zone with lower water vapor content and more stable climatic conditions. Furthermore, the variation in elevation follows a similar pattern as latitude, further validating the superior accuracy and suitability of ERA5 reanalysis data in Inner Mongolia. The above analysis indicates that latitude and elevation are crucial factors influencing the accuracy of PWV retrieval.

To further investigate the spatiotemporal distribution characteristics of PWV, a seasonal comparative analysis of the spatial distribution of PWV inverted from the three datasets was conducted. The average PWV distribution for the four seasons estimated from GNSS, ERA5, and MERRA-2 is displayed in Fig. 17, and the statistical information is listed in Table 4.

From Fig. 17 and Table 4, it can be seen that the spatial distribution of PWV exhibits distinct arid/humid zones characteristics, which are most evident in MERRA-2. With the increase of water vapor from arid to semi-humid areas, the PWV in semi-humid areas is significantly higher than that in arid and semi-arid areas. This phenomenon is particularly evident in the summer when rainfall is abundant, indicating that it is necessary to divide Inner Mongolia into arid/humid zones. The three types of PWV datasets have the same spatial distribution and temporal trend of PWV inversion, showing good consistency. Overall, the PWV of ERA 5 and MERRA-2 have high accuracy in all four seasons, and the PWV distribution of ERA 5 is more consistent with that of GNSS.

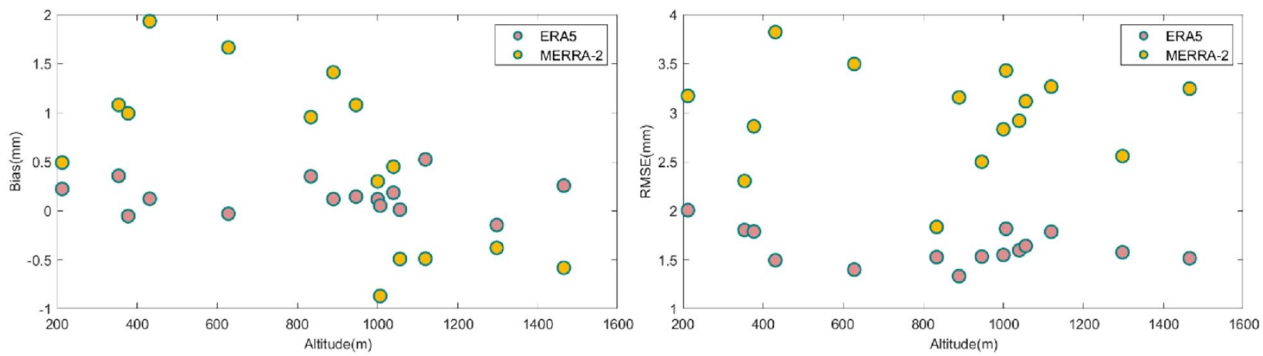

Fig. 16 The variation of annual average bias (left) and RMSE (right) of PWV from ERA5 and MERRA-2 relative to that from GNSS with elevation for various stations in Inner Mongolia from 2019 to 2021

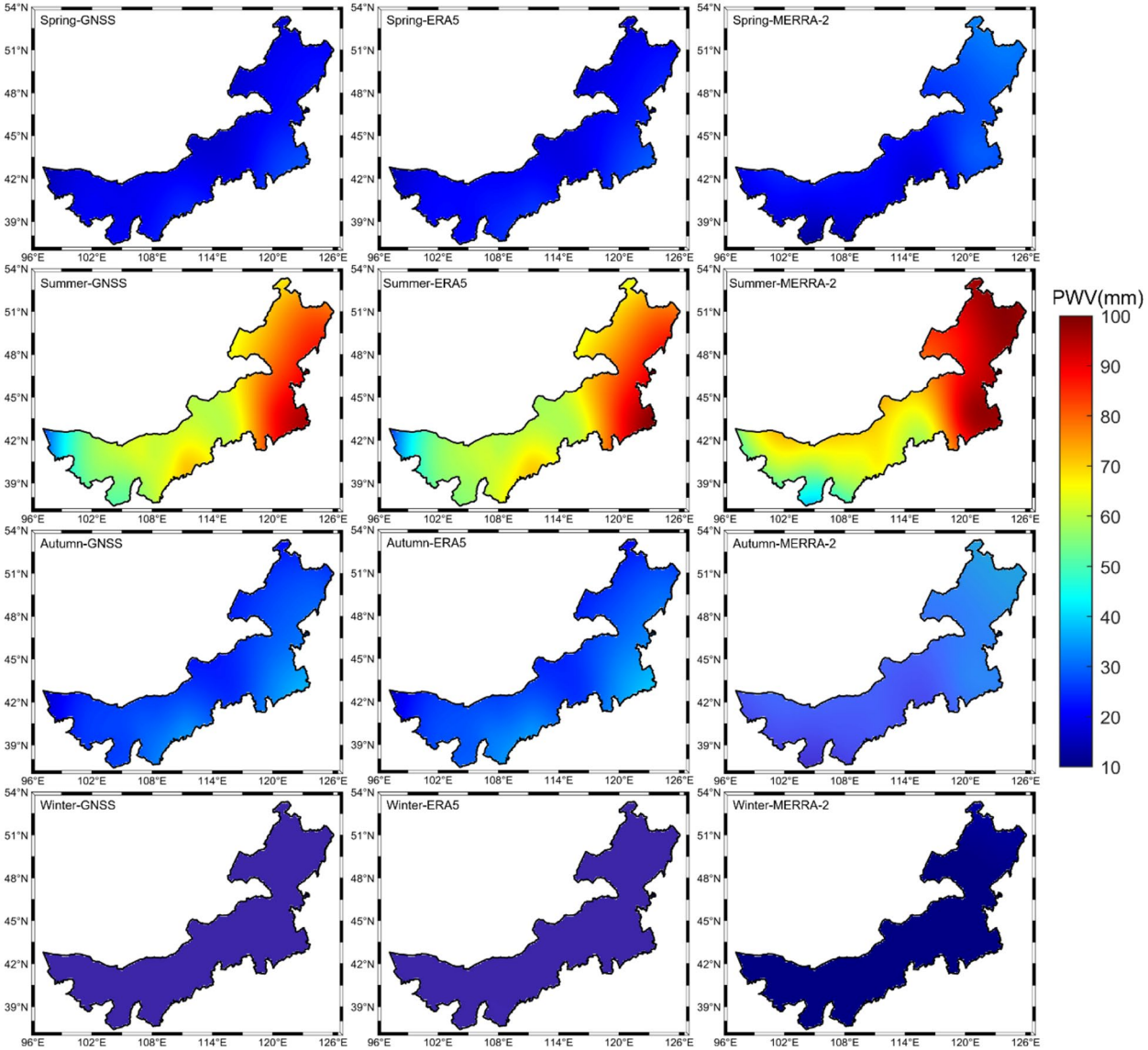

Fig. 17 Distribution of average PWV values in different seasons in Inner Mongolia from 2019 to 2021

Table 4 Statistics of average PWV values in each season from 2019 to 2021 (mm)

Datasets	Spring	Summer	Autumn	Winter
GNSS PWV	21.15	68.59	28.39	7.92
ERA5 PWV	22.17	68.66	29.50	9.04
MERRA-2 PWV	22.80	73.45	28.16	8.10

4 Conclusion

This study aims to comprehensively investigate and analyze the annual, monthly, and diurnal anomaly variations, as well as the spatiotemporal distribution of PWV retrieved from GNSS, ERA5, and MERRA-2 for the Inner Mongolia Region of China. The unique geographical environment in this region, characterized by distinct climates and frequent meteorological disasters, necessitates a thorough understanding of precipitation patterns for effective weather forecasting and disaster warnings. In this study, we utilized ZTD data products of 15 CMONOC GNSS stations in Inner Mongolia from 2019 to 2021 to derive GNSS PWV. The accuracy of GNSS PWV was assessed by comparing with RS PWV. Additionally, we compared the PWVs retrieved from GNSS, ERA5, and MERRA-2, analyzed the annual, monthly, and

diurnal anomaly variations, and the spatiotemporal distribution of PWV. The test results demonstrated that:

(1) The PWV retrieved from GNSS can serve as a reference value in Inner Mongolia to assess PWV obtained from other reanalysis datasets. The reliability of GNSS PWV in Inner Mongolia was validated by RS PWV. The evaluation results indicate that GNSS PWV and RS PWV showed good consistency. The average bias and RMSE of the 4 stations were −0.68 and 2.17 mm, respectively, and the correlation coefficients were all above 0.9.
(2) PWV of EAR5 and MERRA-2 are of relatively high accuracy in the region, with the former higher than the later. The annual average bias of PWV from ERA5 and MERRA-2 were 0.17 and 0.39 mm, and the annual average RMSE were 1.63 and 2.99 mm, respectively. This study of annual variations indicated that the semi-humid zone exhibited a larger annual average bias and RMSE compared to the arid and semi-arid zones.
(3) The monthly average PWV retrieved by ERA5 and MERRA-2 were in good agreement with the GNSS PWV, exhibiting significant seasonal variations. PWV values reached their maximum in summer due to abundant precipitation and significant water vapor changes, while in winter, with cold and dry conditions, water vapor fluctuations were milder, resulting in the minimum PWV values. The monthly average bias and RMSE also showed significant seasonality, with ERA5 PWV having a relatively smaller seasonal impact on accuracy.
(4) The average diurnal anomaly variations of PWV of three datasets in the time series exhibited a similar trend on different stations, indicating good consistency. The diurnal anomaly variations in different arid/humid zones all remained in the range of −0.6–0.6 mm. PWV of ERA5 showed higher consistency with that of GNSS about diurnal anomaly amplitude and phase compared to that of MERRA-2 for the higher spatiotemporal resolution of EAR5. This suggests that ERA5 is more suitable for making research about the diurnal anomaly variations of atmospheric water vapor in Inner Mongolia.
(5) All three datasets exhibited significant seasonal variations in time, with the most pronounced effect observed during the rainfall-abundant summer season. Regarding spatial distribution, latitude, and elevation were important factors that influence the accuracy of PWV inversion.

In conclusion, the comparative analysis of PWV retrieved by GNSS, ERA5, and MERRA-2 in Inner Mongolia indicates good overall consistency. This study will be helpful to the study of the meteorological natural disaster formation, regularity, monitoring, and warning for the Inner Mongolia region.

Acknowledgements
The authors would like to thank the National Oceanic and Atmospheric Administration (NOAA) for providing the radiosonde data and CMONOC for providing the GNSS data. The reanalysis data, namely, the ERA5 and MERRA-2 products, are provided by the ECMWF and NASA, respectively.

Author contributions
QB: visualization, writing—original draft. QLK: conceptualization, methodology, writing review. XLM, WC and JSD: revising the paper and providing critical feedback. YQH: conceptualization, validation, investigation. MQL and QL: validation, review and editing. All authors read and approved the final manuscript.

Funding
This work was supported by the National Natural Science Foundation of China (Grant No. 42374038, 42271436), the Shandong Natural Science Foundation of China (Grant No. ZR2023MD072, ZR2021MD030), a Project of Shandong Province Higher Education Science and Technology Program (Grant No. J17KA077), and Talent introduction plan for Youth Innovation Team in universities of Shandong Province (innovation team of satellite positioning and navigation).

Availability of data and materials
In this experiment, the radiosonde data was obtained from the NOAA (ftp://ftp.ncdc.noaa.gov/pub/data/igra), and the GNSS data from the CMONOC (ftp://ftp.cgps.ac.cn/products/troposphere). The ERA5 data was from the ECMWF (https://cds.climate.copernicus.eu/cdsapp#!/search?text=ERA5/) and the MERRA-2 data from the NASA (https://goldsmr4.gesdisc.eosdis.nasa.gov/data/MERRA2/).

Declarations

Ethics approval and consent to participate
Not applicable.

Consent for publication
Not applicable.

Competing interests
The authors declare that they have no competing interests.

Author details
[1]College of Geodesy and Geomatics, Shandong University of Science and Technology, Qingdao 266590, China. [2]The Department of Land Surveying and Geo-Informatics, The Hong Kong Polytechnic University, Hong Kong, China. [3]Key Laboratory of Geomatics and Digital Technology of Shandong Province, Shandong University of Science and Technology, Qingdao 266590, China. [4]The Seventh Geological Brigade of Hebei Bureau Geology and Mineral Resources Exploration (Xiong'an Geological Survey and Monitoring Center of Hebei Geological and Mineral Exploration and Development Bureau), Baoding 065201, China.

Received: 19 July 2024 Accepted: 17 February 2025
Published online: 03 March 2025

References

Allan R, Soden B (2008) Atmospheric warming and the amplification of precipitation extremes. Science 321:1481–1484. https://doi.org/10.1126/science.1160787

Askne J, Nordius H (1987) Estimation of tropospheric delay for microwaves from surface weather data. Radio Sci 22:379–386. https://doi.org/10.1029/rs022i003p00379

Bevis M, Businger S, Herring T, Rocken C, Anthes R, Ware R (1992) GPS meteorology: remote sensing of atmospheric water vapor using the global positioning system. J Geophys Res 97(D14):15787–15801. https://doi.org/10.1029/92jd01517

Bock O, Parracho A (2019) Consistency and representativeness of integrated water vapour from ground-based GPS observations and ERA-Interim reanalysis. Atmos Chem Phys 19:9453–9468. https://doi.org/10.5194/acp-19-9453-2019

Colman R (2003) A comparison of climate feedbacks in general circulation models. Clim Dynam 20:865–873. https://doi.org/10.1007/s00382-003-0310-z

Dalu G (1986) Satellite remote sensing of atmospheric water vapour. Int J Remote Sens 7:1089–1097. https://doi.org/10.1080/01431168608948911

Frank W (1977) The structure and energetics of the tropical cyclone I. Storm structure. Mon Wea Rev 105(9):1119–1135. https://doi.org/10.1175/1520-0493(1977)105%3c1119:tsaeot%3e2.0.co;2

Gelaro R, McCarty W, Suárez M, Todling R, Molod A, Takacs L, Randles C, Darmenov A, Bosilovich M, Reichle R, Wargan K, Coy L, Cullather R, Draper C, Akella S, Buchard V, Conaty A, Silva A, Gu W, Kim G, Koster R, Lucchesi R, Merkova D, Nielsen J, Partyka G, Pawson S, Putman W, Rienecker M, Schubert S, Sienkiewicz M, Zhao B (2017) The modern-era retrospective analysis for research and applications, version 2 (MERRA-2). J Clim 30(14):5419–5454. https://doi.org/10.1175/jcli-d-16-0758.1

Gui K, Che H, Chen Q, Zeng Z, Liu H, Wang Y, Zheng Y, Sun T, Liao T, Wang H, Zhang X (2017) Evaluation of radiosonde, MODIS-NIR-Clear, and AERONET precipitable water vapor using IGS ground-based GPS measurements over China. Atmos Res 197:461–473. https://doi.org/10.1016/j.atmosres.2017.07.021

He Q, Zhang K, Wu S, Zhan Q, Wang X, Shen Z, Li L, Wan M, Liu X (2019) Real-time GNSS-derived PWV for typhoon characterizations: a case study for super typhoon mangkhut in Hong Kong. Remote Sens 12:104. https://doi.org/10.3390/rs12010104

Hersbach H, Bell B, Berrisford P, Hirahara S, Horányi A, Muñoz-Sabater J, Nicolas J, Peubey C, Radu R, Schepers D, Simmons A, Soci C, Abdalla S, Abellan X, Balsamo G, Bechtold P, Biavati G, Bidlot J, Bonavita M, Chiara G, Dahlgren P, Dee D, Diamantakis M, Dragani R, Flemming J, Forbes R, Fuentes M, Geer A, Haimberger L, Healy S, Hogan R, Holm E, Janisková M, Keeley S, Laloyaux P, Lopez P, Lupu C, Radnoti G, Rosnay P, Rozum I, Vamborg F, Villaume S, Thepaut J (2020) The ERA5 global reanalysis. Q J R Meteorol Soc 146(730):1999–2049. https://doi.org/10.1002/qj.3803

Huang L, Guo L, Liu L, Chen H, Chen J, Xie S (2020) Evaluation of the ZWD/ZTD values derived from MERRA-2 global reanalysis products using GNSS observations and radiosonde data. Sensors 20(22):6440. https://doi.org/10.3390/s20226440

Huang L, Mo Z, Xie S, Liu L, Chen J, Kang C, Wang S (2021a) Spatiotemporal characteristics of GNSS-derived precipitable water vapor during heavy rainfall events in Guilin, China. Satell Navig 2(1):1–17. https://doi.org/10.1186/s43020-021-00046-y

Huang L, Mo Z, Liu L, Zeng Z, Chen J, Xiong S, He H (2021b) Evaluation of hourly PWV products derived from ERA5 and MERRA-2 over the Tibetan Plateau using ground-based GNSS observations by two enhanced models. Earth Space Sci 8(5) e2020EA001516. https://doi.org/10.1029/2020ea001516

Huang L, Fang X, Zhang T, Wang H, Cui L, Liu L (2022a) Evaluation of surface temperature and pressure derived from MERRA-2 and ERA5 reanalysis datasets and their applications in hourly GNSS precipitable water vapor retrieval over China. Geodesy Geodyn 14(2):111–120. https://doi.org/10.1016/j.geog.2022.08.006

Huang L, Wang X, Xiong S, Li J, Liu L, Mo Z, Fu B, He H (2022b) High-precision GNSS PWV retrieval using dense GNSS sites and in-situ meteorological observations for the evaluation of MERRA-2 and ERA5 reanalysis products over China. Atmos Res 276:106247. https://doi.org/10.1016/j.atmosres.2022.106247

Janssen V, Ge L, Rizos C (2004) Tropospheric corrections to SAR interferometry from GPS observations. GPS Sol 8:140–151. https://doi.org/10.1007/s10291-004-0099-1

Jiang P, Ye S, Chen D, Liu Y, Xia P (2016) Retrieving precipitable water vapor data using GPS zenith delays and global reanalysis data in China. Remote Sens 8(5):389. https://doi.org/10.3390/rs8050389

King M, Kaufman Y, Menzel W, Tanre D (1992) Remote sensing of cloud, aerosol, and water vapor properties from the moderate resolution imaging spectrometer (MODIS). IEEE Trans Geosci Remote Sens 30(1):2–27. https://doi.org/10.1109/36.124212

Landskron D, Böhm J (2018) Refined discrete and empirical horizontal gradients in VLBI analysis. J Geodesy 92:1387–1399. https://doi.org/10.1007/s00190-018-1127-1

Li Z, Muller J, Cross P (2003) Comparison of precipitable water vapor derived from radiosonde, GPS, and moderate-resolution imaging spectroradiometer measurements. J Geophys Res 108:4651. https://doi.org/10.1016/j.asr.2022.03.035

Liu Z, Huang L, Liu L, Huang L, Guo X, Liao F (2023) Accuracy analysis of ERA5 and MERRA-2 atmospheric precipitable water in Xinjiang. J Guilin Univ Technol 1–9

Mo Z, Zeng Z, Huang L, Liu L, Huang L, Zhou L, Ren C, He H (2021) Investigation of Antarctic precipitable water vapor variability and trend from 18 year (2001 to 2018) data of four reanalyses based on radiosonde and GNSS observations. Remote Sens 13(19):3901. https://doi.org/10.3390/rs13193901

Namaoui H, Kahlouche S, Belbachir AH, Malderen RV, Brenot H, Pottiaux E (2017) GPS water vapor and its comparison with radiosonde and ERA-Interim data in Algeria. Adv Atmos Sci 34:623–634. https://doi.org/10.1007/s00376-016-6111-1

Niell A, Coster A, Solheim F, Mendes V, Toor P, Langley R, Upham C (2001) Comparison of measurements of atmospheric wet delay by radiosonde, water vapor radiometer, GPS, and VLBI. J Atmos Ocean Technol 18(6):830–850. https://doi.org/10.1175/1520-0426(2001)018%3c0830:comoaw%3e2.0.co;2

Ren D, Wang Y, Wang G, Liu L (2022) Fusion of CMONOC and ERA5 PWV products based on backpropagation neural network. Remote Sens 14:3750. https://doi.org/10.3390/rs14153750

Rocken C, Van Hove T, Ware R (1997) Near real-time GPS sensing of atmospheric water vapor. Geophys Res Lett 24(24):3221–3224. https://doi.org/10.1029/97gl03312

Saastamoinen J (1972) Atmospheric correction for the troposphere and stratosphere in radio ranging satellites. Geophys Monogr Ser 15:247–251. https://doi.org/10.1029/GM015p0247

Ssenyunzi R, Oruru B, Dujanga F, Realini E, Barindelli S, Tagliaferro G, Engeln A, Giesen N (2020) Performance of ERA5 data in retrieving precipitable water vapour over east african tropical region. Adv Space Res 65(8):1877–1893. https://doi.org/10.1016/j.asr.2020.02.003

Wang J, Zhang L (2008) Systematic errors in global radiosonde precipitable water data from comparisons with ground-based GPS measurements. J Clim 21(10):2218–2238. https://doi.org/10.1175/2007jcli1944.1

Wang X, Zhang K, Wu S, Fan S, Cheng Y (2016) Water vapor-weighted mean temperature and its impact on the determination of precipitable water vapor and its linear trend. J Geophys Res Atmos 121(2):833–852. https://doi.org/10.1002/2015jd024181

Wang Y, Yang K, Pan Z, Qin J, Chen D, Lin C, Chen Y, Lazhu Tang W, Han M, Lu N, Wu H (2017) Evaluation of precipitable water vapor from four satellite products and four reanalysis datasets against gps measurements on the Southern Tibetan Plateau. J Clim 30(15):5699–5713. https://doi.org/10.1175/jcli-d-16-0630.1

Wang S (2021) Research on accuracy evaluation and model establishment of ZTD/PWV based on GNSS and reanalysis. Shandong University. https://doi.org/10.27272/d.cnki.gshdu.2021.000305

Wang S, Xu T, Nie W, Jiang C, Yang Y, Fang Z, Li M, Zhang Z (2020) Evaluation of precipitable water vapor from five reanalysis products with ground-based GNSS observations. Remote Sens 12(11):1817. https://doi.org/10.3390/rs12111817

Xu Y, Chen X, Liu M, Wang J, Zhang F, Cui J, Zhou H (2022) Spatial-temporal relationship study between NWP PWV and precipitation: a case study of 'July 20' heavy rainstorm in Zhengzhou. Remote Sens 14(15):3636. https://doi.org/10.3390/rs14153636

Yu S, Liu L (2009) Validation and analysis of the water-vapor-weighted mean temperature from Tm-Ts relationship. Geom Inform Sci Wuhan Univ 34(6):741–744. https://doi.org/10.1073/pnas.73.5.1730

Zeng Z, Mao F, Wang Z, Guo J, Gui K, An J, Yim S, Yang Y, Zhang B, Jiang H (2019) Preliminary evaluation of the atmospheric infrared sounder water vapor over China against high-resolution radiosonde measurements. J Geophys Res Atmos 124(7):3871–3888. https://doi.org/10.1029/2018jd029109

Zhang Q, Ye J, Zhang S, Han F (2018a) Precipitable water vapor retrieval and analysis by multiple data sources: ground-based GNSS, radio occultation, radiosonde, microwave satellite, and NWP reanalysis data. J Sensors 2018:1–13. https://doi.org/10.1155/2018/3428303

Zhang Y, Xu J, Yang N, Lan P (2018b) Variability and trends in global precipitable water vapor retrieved from COSMIC radio occultation and radiosonde observations. Atmosphere 9(5):174. https://doi.org/10.3390/atmos9050174

Zhang W, Zhang H, Liang H, Lou Y, Cai Y, Cao Y, Zhou Y, Liu W (2019a) On the suitability of ERA5 in hourly GPS precipitable water vapor retrieval over China. J Geodesy 93(10):1897–1909. https://doi.org/10.1007/s00190-019-01290-6

Zhang Y, Cai C, Chen B, Dai W (2019b) Consistency evaluation of precipitable water vapor derived from ERA5, ERA-Interim, GNSS, and radiosondes over China. Radio Sci 54(7):561–571. https://doi.org/10.1029/2018rs006789

Zhang H, Yuan Y, Li W, Ji D, Lv M (2021) Implementation of ready-made hydrostatic delay products for timely GPS precipitable water vapor retrieval over complex topography: a case study in the Tibetan Plateau. IEEE J Select Top Appl Earth Observ Rem Sens 14:9462–9474. https://doi.org/10.1109/JSTARS.2021.3111910

Zhao T, Fu C, Ke Z, Guo W (2010) Global atmosphere reanalysis datasets: current status and recent advances. Adv Earth Sci 25(3):241–254. https://doi.org/10.11867/J.ISSN.1001-8166.2010.03.0241

Zhao Q, Yang P, Yao W, Yao Y (2019) Hourly PWV dataset derived from GNSS observations in China. Sensors 20(1):231. https://doi.org/10.3390/s20010231

Zhao S, Zhou Q, Wang W, Wu Y (2022) Dry and wet climate characteristics in inner mongolia based on SPI index. J China Inst Water Resour Hydropower Res20(01):10–19. https://doi.org/10.13244/j.cnki.jiwhr.20210208

Publisher's Note